



Depositional environments and source rock potential from molecular to basin scales: An example from the Middle to Upper Cretaceous succession, Abu Gharadig Basin, Egypt

Haytham El Atfy^{1,2} · Bandar I. Ghassal³ · Linda Burnaz⁴ · Salah Y. El Beialy²

Received: 2 December 2023 / Accepted: 5 August 2024

© Deutsche Geologische Gesellschaft - Geologische Vereinigung DGGV e.V. 2024

Abstract

We present a case study of high-resolution screening and integration of palynological and organic geochemical methodologies in the TSW-21 well in the Abu Gharadig Basin, north Western Desert of Egypt. A total of 84 cores and cuttings samples were analyzed for TOC wt%, Rock–Eval pyrolysis, molecular geochemistry, vitrinite reflectance ($R_o\%$), and palynology. The categorization of dispersed organic matter in palynological macerals shows that it differs not only in palynofacies properties but also in distinct palynomorph characteristics (mainly abundance, diversity, marine versus non-marine, and preservation). The work highlights the value of integrating optical and geochemical methods in screening hydrocarbon source rock potential, and the implications for kerogen examination and the reconstruction of depositional environments. In the present study, data indicate a marine, near-shore depositional environment of the middle Cretaceous Bahariya Formation, and more open-marine conditions for the overlying strata of the Upper Cretaceous Abu Roash Formation. A variety of kerogen types (II/III, II, III, and IV) is predominant in the Bahariya Formation and is mainly gas-prone (highly phytoclastic and rich in amorphous organic matter [AOM]). In contrast, the Abu Raoash Formation yielded highly oil-prone Type II > I kerogen (AOM-rich). Thermal maturity proxies including Rock–Eval pyrolysis (T_{max}), $R_o\%$, and Spore Coloration Index (SCI) reveal that the Bahariya and Abu Raoash formations are immature.

Keywords Palynofacies · Organic geochemistry · Rock–Eval · North Western Desert · Egypt

Introduction

Several physical and chemical factors control organic matter richness (organic productivity) and preservation (Ghassal and El Atfy 2023). Organic matter (OM) productivity in marine deposits is controlled by chemical factors, encompassing the availability of nutrients, oxygen, and water

salinity, whereas relevant physical factors are sunlight intensity, climate, and geographical location. The preservation of OM is mainly influenced by primary productivity, anoxicity, sedimentation rates, energy (e.g., currents), and mineral surface area. These factors need to be discussed when evaluating source rock potential.

The study of particulate organic matter (POM) preserved in palynological macerations has an essential role in the identification of depositional environments. Palynologists usually classify POM into structured (including palynomorphs) and amorphous organic matter (AOM) components. In a different context, organic geochemists commonly lump all these elements into the generalized term OM (Huc 1988), even if they comprise various chemical structures as reflected in their pyrolysis–gas chromatography patterns (Gastaldo 1994 and references therein). However, some OM categorizations based on different geochemical analytical methods cannot be overlooked. Morphological categorization of these palynological OM particles undoubtedly contributes to a better understanding of their characters.

✉ Haytham El Atfy
El-Atfy@daad-alumni.de

¹ Palaeobotany Group, Institute of Geology and Palaeontology, University of Münster, 48149 Münster, Germany
² Geology Department, Faculty of Science, Mansoura University, Mansoura 35516, Egypt
³ Geology Technology Division, EXPEC Advanced Research Center, 31311 Saudi Aramco, Dhahran, Saudi Arabia
⁴ Institute of Organic Biogeochemistry in Geo-Systems, Energy and Mineral Resources Group (EMR), RWTH Aachen University, 52064 Aachen, Germany

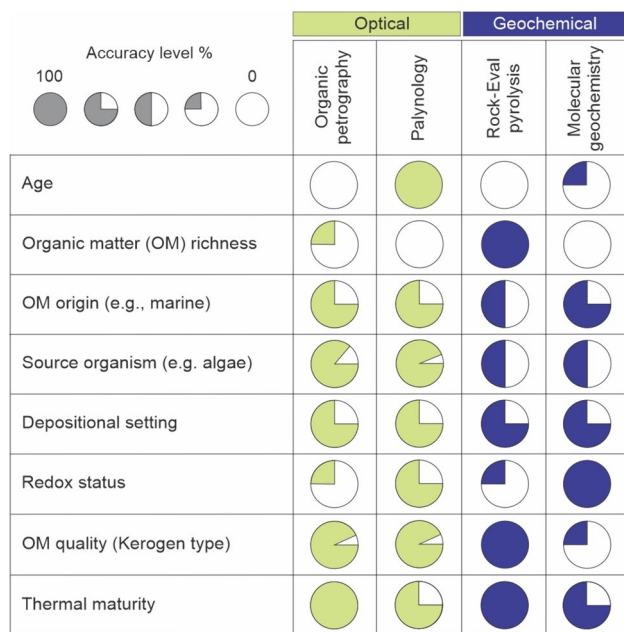


Fig. 1 Diagram showing the effectiveness of this study's optical and geochemical source rock evaluation methods. The shaded pie charts represent schematic depictions of levels of accuracy between the different techniques

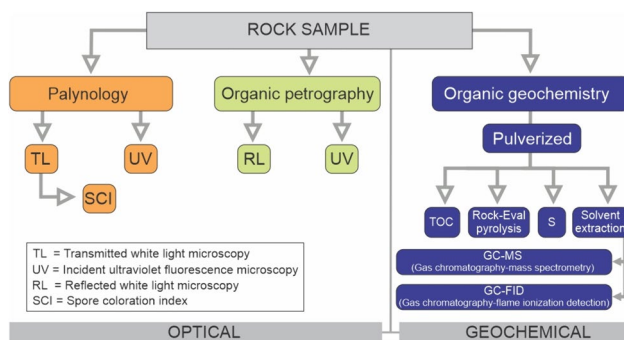


Fig. 2 Source rock analysis workflow used in this study, displaying the optical (palynology, organic petrography) and organic geochemical techniques for analyzing organic matter

Moreover, Rock–Eval pyrolysis data are unreliable for samples with low to moderate total organic carbon (TOC) due to the retained hydrocarbons in the mineral milieu (e.g., Grohmann et al. 2018); in addition, there can be attendant flawed readings of hydrogen and oxygen indices.

The integration of optical (i.e., palynology and organic petrology) and organic geochemical methods (Fig. 1) provides convincing data for the interpretation of kerogen types, petroleum source rock potential, and paleoenvironments. High-resolution screening via such approaches (Fig. 2) provides a comprehensive understanding of source rock richness, quality, and thermal maturity, and it clarifies the

process of changes in these properties. Figure 1 provides a general overview of the methods used in this study. This analytical framework has previously been tested in numerous petroleum basins globally and has been accepted as a valid approach (e.g., Mendonça Filho et al. 2012; Ghassal et al. 2018; Țabără et al. 2022; El Atfy et al. 2023a).

The Upper Cretaceous strata in the north Western Desert of Egypt contain OM-rich units. Due to their significant contribution as a source (and also reservoirs) of hydrocarbons, these deposits have been intensely investigated (cf. El Atfy et al. 2023a). The research reported here is aimed at establishing a fingerprint for OM deposition in each rock unit studied. This has involved high-resolution examination of the optical and geochemical data for each sample to produce reliable depositional reconstructions. It is hoped that the present study will enable a better understanding of successional changes in the Abu Gharadig Basin and will prove to be of value for comparative studies of temporally equivalent localities from the north Western Desert.

Methods

Samples

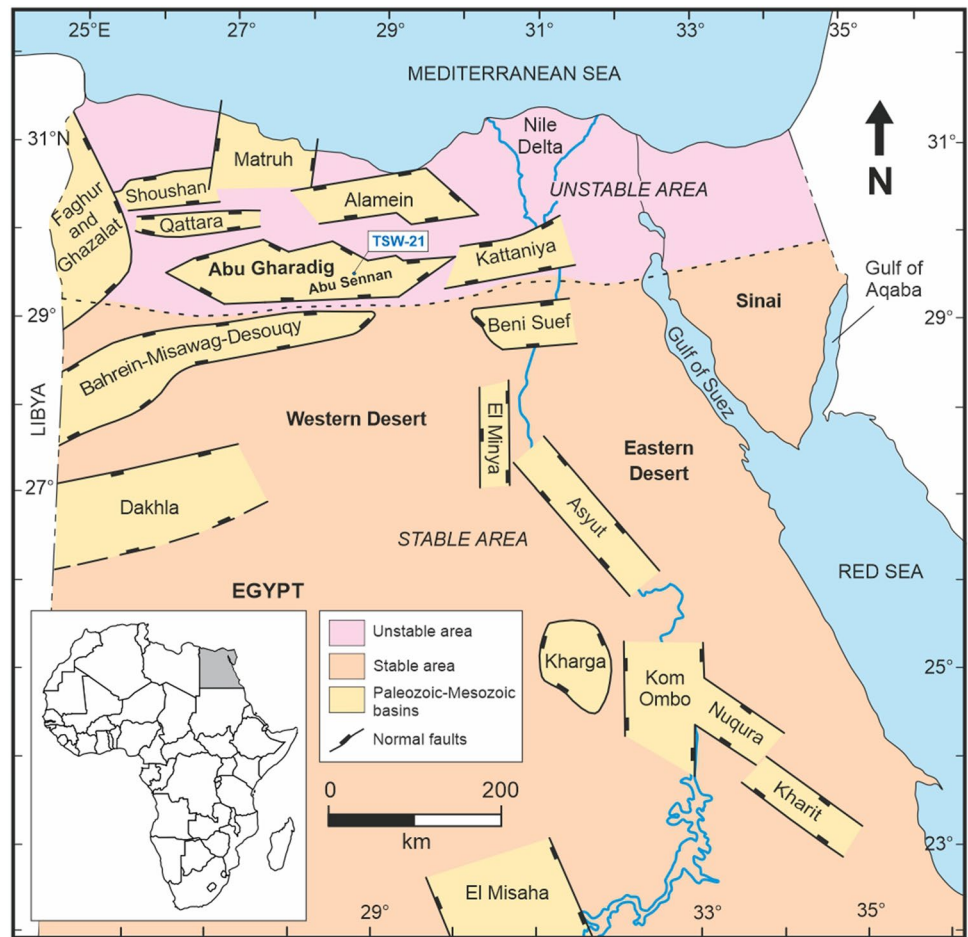
A total of 84 cores and cuttings samples from the Bahariya and Abu Roash formations were selected for the study (Supplementary data; Table 1) from the South West Abu Senan-21 (TSW-21) well (Fig. 3). The well is located in the southern Abu Gharadig Basin (Latitude 29° 34' 09.49" E, Longitude 28° 36' 10.600" N) and reached a total depth of 2222 m in the Kharita Formation. The investigated section ranges in depth from 1542 to 2188 m.

Palynology

Thirty-five (10 cores and 25 cuttings) of 84 samples were prepared palynologically, representing all rock units (Supplementary data; Table 1). The processed samples comprised 13 from the Bahariya Formation, 9 from the Abu Roash G, 2 from the Abu Roash F, 7 from the Abu Roash E, 2 from the Abu Roash C, and 1 from the Abu Roash A members.

An aliquot of approximately 10 to 15 g per sample was prepared according to conventional maceration techniques, including cold HCl and HF acid treatments with no alkaline or oxidation processes (e.g., Riding 2021). After neutralization, the residues were sieved through a 10 μm nylon mesh and strewn-mounted on glass slides using Elvacite® 2044. The mounted slides were viewed under transmitted white light and incident fluorescence microscopy to provide a qualitative description of the retrieved organic particles; quantitative data are presented in Supplementary data: Table 2. Photomicrographs were taken with a mounted Canon EOS-R

Fig. 3 Sedimentary basins of Egypt (modified after Moustafa et al. 2003), and the location of the studied borehole



digital camera using either a Leica DM5500 B microscope with normal transmitted and incident UV light or a Leica Diaplan microscope with Nomarski interference contrast. For fluorescence setup, the Leica DM5500 B microscope is equipped with a motorized excitation manager (EXMAN) to control the fluorescence emission when using filter cube I3 (FLUO; Excitation Filter 8P450/490, a Dichromatic Mirror 510 and a Suppression Filter LP 515) by pushing the TL/IL button. Many images were stacked (using the Helion Focus software suite) from individual shots from different focal planes aided by Leica LAS-X software to enhance image quality (cf. Kerp and Bomfleur 2011).

Organic particles were categorized into three main groups (Batten 1996): (1) palynomorphs; (2) structured OM (both phytoclasts and zooclasts); and (3) structureless OM incorporating AOM, gelified matter, resin, amber, and solid bitumen. Consequently, three main subdivisions of palynomorphs, phytoclasts, and AOM were determined. Their variations are traced through the sections to elucidate the paleoenvironmental conditions in the investigated intervals (Supplementary data; Tables 1–2).

Organic petrology

Four cuttings and eight core samples were prepared by grinding and polishing to recognized standards (ISO 7404–2, 2009a; ASTM-D2797/D279 2021) as described in Burnaz et al. (2023). Vitrinite reflectance was measured on a Zeiss Axio Scope A1 microscope equipped with a Basler Scout monochrome digital camera, a Zeiss EC Epiplan-NEOFLUAR 50x/1.0 oil immersion objective, and a 546 nm interference filter. Random vitrinite reflectance (R_o %) measurement and maceral observation and documentation were conducted using the Diskus-Fossil software suite from Hilgers Technisches Büro under non-polarized light, consistent with ISO 7404–5 (2009b). Qualitative maceral identification was conducted using the Zeiss Axio Image.M2m equipped with a Basler Scout color camera. For fluorescence observation, an HXP 120 C light source with the fluorescence filter set 09 (Alexa Fluor 488-excitation BP 450–490 nm, beam splitter FT 510 nm, emission LP 515 nm) was used.

Elemental analysis

A total of 84 (72 cuttings and 12 cores) finely ground, air-dried samples were analyzed for elemental composition (Supplementary data; Table 1). Total organic carbon (TOC) and total inorganic carbon (TIC) content was measured using the LiquiTOC II basic unit from Elementar Analysensysteme GmbH with oxygen as the carrier gas. For organic carbon combustion, approximately 100 mg sample material was heated to 550 °C for 600 s, followed by a further temperature increase to 1000 °C, held for 400 s for inorganic carbon oxidation. Released CO₂ was measured using a non-dispersive infrared detector. Carbonate content was estimated, approximately, from TIC and assuming inorganic carbon to be bound in calcite (CaCO₃). This was based on the molar mass relationship of carbon in calcite:

$$(CaCO_3 = TIC * [molar\ mass\ CaCO_3]/[molar\ mass\ C]) \quad (1)$$

Total sulfur (TS) content was measured in 20 samples (Supplementary data; Table 1) using a Leco S200 Determinator. Approximately, 1 g sample material was combusted in a high-frequency induction furnace in an oxidizing environment and the released sulfur (as SO₂) was detected by an infrared cell, indicating the TS content.

Rock–Eval pyrolysis

Rock–Eval pyrolysis was performed on all 84 fine-grained, air-dried samples using the Rock–Eval 6 instrument from Vinci Technologies. Approximately, 100 mg of material was pyrolyzed under a controlled standardized temperature program. Nitrogen was used as the carrier gas, and generated hydrocarbons and CO₂ were detected with a flame ionization detector and an infrared cell, respectively.

The programmed pyrolysis starts with rapid heating to a temperature of 300 °C with an isothermal hold of 3 min, where free hydrocarbons volatilize, detected as S₁ (mg HC/g rock), followed by heating at a rate of 25 °C/min from 300 to 550 °C with the detection of hydrocarbons generated by kerogen cracking, detected as S₂ (mg HC/g rock). The yield of CO₂ from kerogen conversion is recorded during early pyrolysis up to 400 °C, given by S₃ (mg CO₂/g rock). Furthermore, the temperature of the maximum rate of hydrocarbon formation during pyrolysis (T_{max}) was recorded. In addition, the hydrogen index (HI = S₂/TOC × 100 in mg HC/g TOC), the oxygen index (OI = S₃/TOC × 100 in mg CO₂/g TOC), and the production index (PI = S₁/(S₁ + S₂)) were calculated based on the pyrolysis parameters. The Rock–Eval pyrolysis and the derived parameters are described in detail in Behar et al. (2001).

Molecular organic geochemistry

Thirteen finely crushed and homogenized samples were extracted by automated accelerated solvent extraction using a DIONEX ASE 150 device from Thermo Scientific Inc. The extracts were dried with Na₂SO₄ and desulfurized by binding elemental sulfur to activated copper. The aliphatic fraction was separated by column chromatography using *n*-pentane. The aliphatic fraction was condensed to approximately 150 µl and analyzed on a Fisons Instruments GC8000 gas chromatograph equipped with a Zebron EB-1 silica column (30 m × 0.25 mm, 0.25 µm film thickness) and a flame ionization detector (GC-FID). Hydrogen was used as a carrier gas at a flow rate of 40 m/s. The injector temperature was set to 270 °C and the heating program started at 60 °C with an isothermal hold of 3 min followed by heating at a rate of 5 °C/min up to 310 °C with a final isothermal hold of 20 min. The chromatograms were used for concentration assessment and the identification of *n*-alkanes and isoprenoids using the Atlas software.

All extracted and fractionated samples were additionally analyzed by gas chromatography coupled to mass spectrometry (GC–MS) on a Finnigan MAT 95Q MS equipped with a Zebron-5 ms capillary column (30 m × 0.25 mm, 0.25 µm film thickness) using helium as a carrier gas. The initial GC temperature was set at 80 °C and held isothermally for 3 min. The temperature increased at a heating rate of 10 °C/min up to 160 °C, followed by a heating rate of 5 °C/min to a final temperature of 320 °C, which was held isothermally for 20 min. Measurements were conducted in full scan mode from 35 to 700 *m/z*.

Peak areas of relevant biomarkers were determined using the Xcalibur software to identify terpanes (*m/z* 191) and steranes (*m/z* 217).

Molecular geochemical parameters

A selection of aliphatic molecular geochemical parameters was employed to characterize source rocks in terms of OM source, paleodepositional environment, and thermal maturity as presented below.

Organic matter source

GC-FID chromatograms were used to qualitatively determine *n*-alkanes and acyclic isoprenoids, pristane (Pr) and phytane (Ph) concentrations. The terrigenous aquatic ratio (TAR) is based on the relative abundance of *n*-alkanes derived predominantly from land-plant (*n*C₂₇, *n*C₂₉, and *n*C₃₁) and aquatic source (*n*C₁₅, *n*C₁₇, and *n*C₁₉) materials (Bourbonniere and Meyer 1996):

$$TAR = \frac{(nC_{27} + nC_{29} + nC_{31})}{(nC_{15} + nC_{17} + nC_{19})} \quad (2)$$

The relative abundances of regular steranes (C_{27} , C_{28} , and C_{29} $\alpha\alpha$ 20S + 20R and $\alpha\beta\beta$ 20S + 20R) and 17 α -hopanes (C_{29} and C_{30} , and C_{31} to C_{33} 22S + 22R) reflect the relative input of organic matter derived from eukaryotic and prokaryotic organisms respectively (Moldowan et al. 1985). Accordingly, high ratios of regular steranes over 17 α -hopanes (steranes/hopanes > 1) indicate marine OM, whereas ratios < 1 suggest a high contribution of terrestrial OM and/or microbially reworked OM. The relative distribution of C_{27} , C_{28} , and C_{29} regular steranes additionally provides information on the source of OM, as empirical studies suggest that C_{27} regular steranes are associated with aquatic OM, whereas C_{29} regular steranes are linked with terrestrial OM (Huang and Meinschein 1979).

Paleodepositional environment

Pr and Ph are mainly derived from the phytol side chains of chlorophyll. Under oxic conditions, the conversion of phytol to Pr is dominant, whereas, under anoxic conditions, further reduction to Ph is the dominant reaction. Thus, the Pr/Ph ratio provides information on paleoredox conditions in the bottom water column and the pore water near the sediment–water interface. Pr/Ph values < 1 indicate anoxic deposition and values > 1 are characteristic for deposition under oxic conditions (Didyk et al. 1978). However, conclusions about paleoredox conditions based on Pr/Ph should be supported by additional geochemical or palynological data, as the ratio can be significantly affected by thermal maturation, source input, and/or paleosalinity.

The presence of gammacerane indicates deposition under water column stratification. This is often associated with hypersaline and highly reducing conditions in the bottom water column (Sinninghe Damsté et al. 1995). The relative abundance of gammacerane is commonly normalized to C_{30} hopane, expressed as the gammacerane index (GI):

$$GI = 10 \times \text{gammacerane} / (\text{gammacerane} + C_{30}\text{hopane}) \quad (3)$$

Furthermore, the ratio of diasteranes to regular steranes (e.g., C_{27} diasterane/regular sterane) provides information on the mineralogy of the sedimentary rock and the paleoredox conditions as the abundance of clays catalyzes the formation of diasterane precursors (Rubinstein 1975). Thus, a low relative abundance of diasteranes indicates an anoxic, clay-poor rock matrix and a high concentration suggests clay-dominant mineralogy.

Thermal maturity

The relative concentrations of isoprenoids and n -alkanes can be used for the assessment of thermal maturity. In this context, the abundance of Pr and Ph relative to nC_{17} and nC_{18} is influenced by the ongoing formation of n -alkanes by kerogen conversion, resulting in a decreasing Pr/ nC_{17} and Ph/ nC_{18} ratio with increasing maturity. In addition, the n -alkane distribution provides information on the thermal maturity stage. This can be explained whereby thermally mature samples generally have a balanced distribution of odd- and even-numbered n -alkanes. The latter is quantified as the Carbon Preference Index (CPI) which can be calculated according to Bray and Evans (1961) as follows:

$$CPI = 2 \left(\frac{nC_{23} + nC_{25} + nC_{27} + nC_{29}}{nC_{22} + 2(nC_{24} + nC_{26} + nC_{28}) + nC_{30}} \right) \quad (4)$$

Thermal maturity parameters based on the relative concentration of certain steranes and terpanes are mainly related to isomerization, with an increasing abundance of the thermally more stable isomers. An example of a sterane maturity proxy is the C_{29} regular sterane (reg. sterane) 20S/(20S + 20R) isomerization ratio, with the isomeric equilibrium reached at values of 0.52 to 0.55, corresponding to peak oil windows at about 0.8% R_o . The C_{30} moretane/hopane thermal maturity ratio is sensitive over a similar thermal maturity range, reaching a minimum of < 0.15 at around 0.7% R_o . The isomerization of 22R to the thermally more stable 22S homohopane isomer reaches its maximum at a lower thermal maturity of about 0.6% R_o . For C_{31} homohopane (C_{31} hop.) isomerization equilibrium 22S/(22S + 22R) ratio is reached at about 0.55. In contrast, the ratio of C_{27} 18 α -trisorneohopane and 17 α -trisorhopane (C_{27} Ts/(Ts + Tm)) is sensitive over a wider thermal maturity range with an endpoint at condensate/wet gas thermal maturity, corresponding to approximately 1.5% R_o (Peters 1998).

Abu Gharadig Basin: a case study (TSW-21 well)

Geological setting and lithostratigraphy

The Abu Gharadig Basin is among the most economic petroleum provinces in Egypt and is located in the northern part of the Western Desert (Fig. 3). The basin represents a part of the northeastern African Craton, which was tectonically active during much of the Paleozoic and Mesozoic (Guiraud and Bosworth 1999; Guiraud et al. 2001). It outlines a Mesozoic E–W trending graben system (Bayoumi 1996) where rifting started during the Late Jurassic, coinciding with the opening of the Neotethys and deep crustal extensions that

affected northern Egypt (Awad 1984; Bayoumi and Lotfy 1989).

Previous studies of the stratigraphic evolution of northern Egypt assumed that Cretaceous sedimentation in the northern part of the Western Desert was mainly controlled by global eustatic sea level and regional tectonics (e.g., Guiraud and Bosworth 1999; Guiraud et al. 2001, 2005). Generally, sedimentation during the Early Cretaceous represents a major regressive phase except for the Aptian time window, when a shallow sea covered North Africa, including the northern Western Desert of Egypt (Guiraud and Bosworth 1999; Guiraud et al. 2001). The Upper Cretaceous strata, on the other hand, witness a major transgressive trend (Said 1990; Deaf et al. 2020; El Atfy et al. 2023b). The Cretaceous strata in Egypt encompass multiple generative source horizons, making them the primary target for exploration (El Atfy et al. 2023a). Those strata are subdivided into a lower clastic unit, represented by the Lower Cretaceous Burg El Arab Formation (comprising from bottom to top: Alam El Bueib, Alamein, Dahab, and Kharita members), and an upper carbonate-dominated unit of Late Cretaceous age that embodies from bottom to top, the Bahariya, Abu Roash, and Khoman formations. The current work focuses mainly on the Bahariya and Abu Roash formations (Fig. 4).

The Bahariya Formation is of early Cenomanian age and witnessed considerable changes in its depositional facies—from fluvial to estuarine to lagoonal sediments—higher in the succession (Dominik 1985). The lithology varies from cross-bedded coarse-grained sandstone at the base, to fossiliferous or sandy dolomite at the top (Awad 1984; Hantar 1990). In the northern Western Desert, the formation was deposited in a near-shore inner shelf environment (e.g., Abdel-Kireem et al. 1996). Conversely, in the south, the formation was deposited in fluvial to estuarine settings (e.g., El Atfy et al. 2023b).

The overlying Abu Roash Formation consists of upper Cenomanian to Coniacian–Santonian deposits that rest conformably on the Bahariya Formation. It represents periods of cyclical marine transgression/regression and comprises seven members, named “G” to “A” from bottom to top. The G Member is late Cenomanian in age and was deposited in a shallow marine context (Abdel-Kireem et al. 1996). The F Member is late Cenomanian/early Turonian in age deposited in a shallow marine environment (Abdel-Kireem et al. 1996; El Beialy et al. 2010a, b; Zobia et al. 2011). It is composed mainly of carbonate interbedded with shale (Abdel-Kireem et al. 1996; Hantar 1990; El Beialy et al. 2010a, b). Its basal part is characterized by a positive $\delta^{13}\text{C}$ isotope excursion reflecting the OAE2 phenomenon (Zobia et al. 2011). The E to B members are Turonian in age but differ in lithology and inferred depositional environments. The regression phase of Abu Roash E Member is dominated by clastic lithologies and acts as a reservoir (Ahmed 2008).

Previous palynological studies reported the ubiquity of the freshwater green alga *Pediastrum* at the base of the member, reflecting a fall in sea level and the increased influence of terrestrial OM (e.g., Abdel-Kireem et al. 1996; Zobia et al. 2011). The D and B members were deposited in periods of marine transgression marked by carbonates, unlike the C Member, which is characterized by regression phase clastic facies (Hantar 1990; Ahmed 2008). The Abu Roash A Member was laid down as transgression facies in a shallow water, clastic middle shelf environment (Abdel-Kireem et al. 1996) during the Coniacian–Santonian (Said 1990; Ahmed 2008).

Results

Palynological composition

The palynomorph and palynofacies content of each rock unit are described below. The kerogen (palynofacies) particles recorded from the studied rock units are moderately preserved and diverse.

Bahariya Formation

Palynologically, 13 samples from the Bahariya Formation were investigated (Supplementary data; Table 1). The sequence consisted mainly of phytoclasts, including cuticle, wood, and other plant remains that were mostly well preserved, lath-shaped to equidimensional, translucent to brown-colored, sometimes opaque, and rarely biodegraded (Fig. 5). AOM was generally yellow to yellowish-brown and granular, incorporating occasional resin shards, and appeared fluorescent in incident blue light microscopy (Fig. 5). Palynomorphs were diverse and comprised algae (e.g., *Botryococcus*), sporomorphs, and marine elements. Sporomorph taxa embraced spores such as *Cicatricosisporites minutaestriata*, *Cicatricosisporites* spp., *Concavisorites* spp., *Cyathidites australis*, *Cyathidites minor*, *Deltoidospora* spp., *Laevigatosporites* sp., *Leptolepidites* sp., *Matonisporites* sp., *Triplanosporites* spp., *Verrucatosporites* sp., and unidentified forms, as well as aquatic fern spores including *Ariadnaesporites* spp., *Crybelosporites pannuceus*, and *Gabonisporis* sp. Gymnosperm pollen included *Araucariacites* sp., *Balmeiopsis limbatus*, *Classopollis brasiliensis*, *Classopollis* spp., *Cycadopites* spp., *Eucommiidites troedssonii*, ephedroids (*Ephedripites*, *Equisetosporites*, *Steevesipollenites*), *Exesipollenites* sp., *Inaperturopollenites* sp. and *Monosulcites* sp. and rare representatives of so-called elaterate pollen (*Elateroplicites africaensis* and *Elaterosporites klaszii*). The dominant element, however, was the *Afropollis* complex, which comprised *Afropollis jardinus*, *Afropollis kahramanensis* and *Afropollis* spp. Angiosperm pollen formed the most

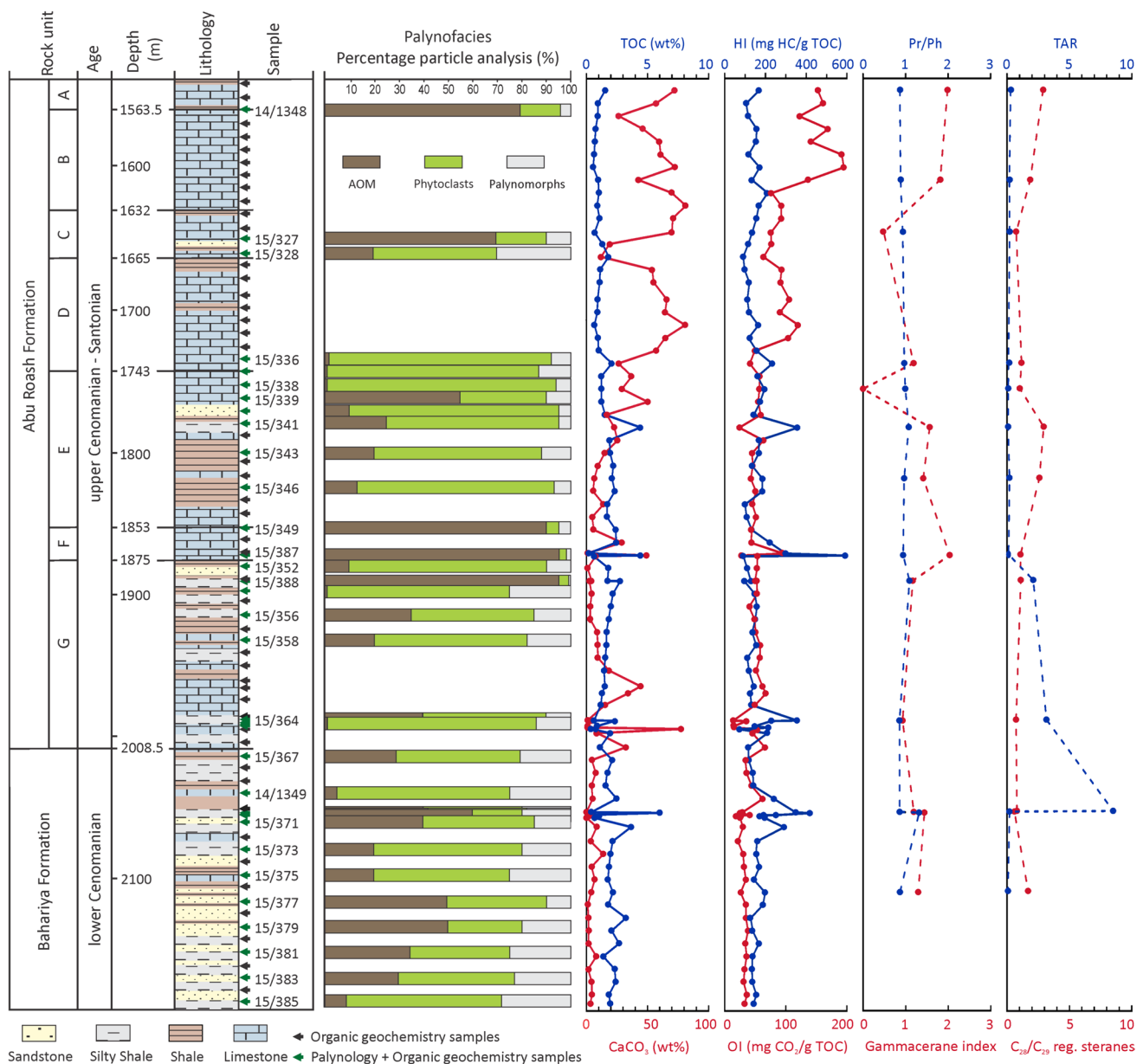


Fig. 4 Lithology, palynofacies data, elemental data (TOC and CaCO₃), Rock-Eval pyrolysis parameters (HI and OI), and molecular geochemical ratios (Pr/Ph, Gammacerane index, TAR and C₂₈/

C₂₉ regular steranes) of the Bahariya and Abu Roash formations in the TSW-21 well, north Western Desert, Egypt. Note that CaCO₃ is calculated from total inorganic carbon

diverse palynomorph group. It encompassed *Cretacaeiporits aegyptiaca*, *Cretacaeiporits densimurus*, *Cretacaeiporits muelleri*, *Cretacaeiporits polygonalis*, *Cretacaeiporits scabratus*, *Dichastopollenites dunveganensis*, *Foveomorphomonocolpites rashadi*, *Foveotricolpites* sp., *Foveotricolpites giganteus*, *Monocolpopollenites* spp., *Nyssapollenites* sp., *Pennipollis peroreticulatus*, *Perinopollenites halonatus*, *Retitricolpites* sp., *Retimonocolpites variplicatus*, *Retimonocolpites* spp., *Rousea* sp., *Stellatopollis* sp., *Tricolpites* spp., and unidentified forms. Marine

elements comprised mainly dinoflagellate cysts dominated by *Subtilisphaera* and hosted the occasional presence of *Circulodinium distinctum*, *Cleistosphaeridium* sp., *Coronifera albertii*, *Cribropieridinium edwardsii*, *Florentinia mantellii*, acritarchs (*Micrhystridium* spp.), leiosphaerids, and microforaminiferal linings (Fig. 5g, i).

Abu Roash Formation

The Abu Roash G Member was covered by 9 samples (Supplementary data; Table 1), which were all palyniferous

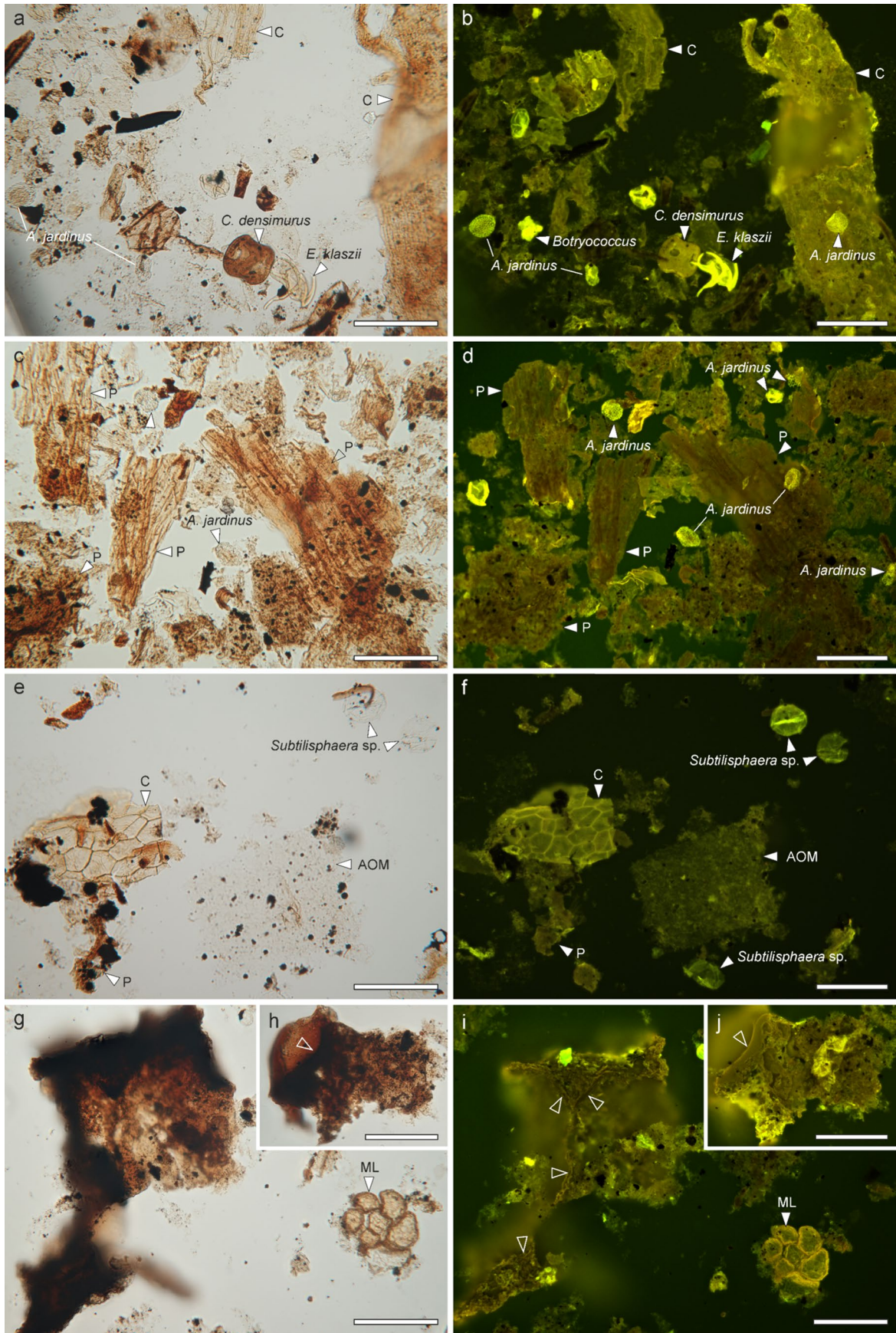


Fig. 5 OM assemblage characteristic for the Bahariya Formation in the TSW-21 well, north Western Desert, Egypt as seen under transmitted white light and incident UV fluorescence microscopy. **a, b** Representative palynofacies associations composed mainly of non-marine particles and palynomorphs including algae such as *Botryococcus*. Index palynomorphs are *Afropollis jardinus*, *Cretacaeiporitis densimurus*, and *Elaterosporites klaszii* (Sample 15/385). **c, d** Lath-shaped phytoclast-dominated assemblages, composed of plant tissues (P), mostly degraded, with the notable occurrence of *A. jardinus* (Sample 15/392). **e, f** *Subtilisphaera*-dominated palynofacies together with well-preserved cuticles (C) show cellular internal structure and sheet-like fluorescent AOM (Sample 15/373). **g–j** Biodegraded phytoclast particles with fluorescent coiled planispiral microforaminiferal linings (ML). The relics of cellular structures in biodegraded phytoclasts could be seen under incident UV light as highlighted with arrows in **i–j** (Sample 15/377). Scale bars: 100 μm

apart from 2 core samples (15/388 and 15/392) that were barren and featured little organic matter. This interval was mostly phytoclast-dominated, with variable percentages of remains diluted in some strata with AOM and palynomorphs (Fig. 6). Phytoclasts were generally well preserved with recognizable cell structures, lath-shaped to equidimensional, translucent to brown-colored, sometimes opaque, rarely biodegraded, and included cuticles, wood, and tracheids. Palynomorphs were diverse and dominated by algae (*Botryococcus*, *Pediastrum*) and sporomorphs, while the increase in marine elements—dinoflagellates (especially *Subtilisphaera* spp.), acritarchs, leiosphaerids, and microforaminiferal linings—was notable. Typical spore taxa included *Cicatricosisporites* spp., *Concavisporites* sp., *Cyathidites australis*, *Deltoidospora* spp., *Leptolepidites psarosus*, and *Triplanosporites* spp., and unidentified forms as well as spores of aquatic ferns, e.g., *Ariadnaesporites*, *Crybelosporites pannuceus*, and *Gabonisoris* spp. Gymnosperm pollen featured *Araucariacites* sp., *Balmeiopsis limbatus*, *Classopollis* spp., *Cycadopites* spp., *Eucommiidites troedssonii*, ephedroids (*Ephedripites*, *Equisetosporites*, *Steevesipollenites*), *Inaperturopollenites* sp. and *Monosulcites* sp. *Afropollis* spp. also occur. The angiosperm pollen taxa comprised *Cretacaeiporitis aegyptiaca*, *Cretacaeiporitis densimurus*, *Cretacaeiporitis muelleri*, *Cretacaeiporitis polygonalis*, *Cretacaeiporitis scabratus*, *Foveotricolpites* sp., *Foveotricolpites giganteus*, *Foveotricolpites gigantoreticulatus*, *Perinopollenites halonatus*, *Retitricolpites* sp., *Retimonocolpites* spp., *Rousea* sp., and *Tricolpites* spp. The enigmatic non-pollen palynomorph *Chomotriletes* sp. (Euglenophyceae; Schootbrugge et al. 2024) and *Incertae sedis* (*Reyrea polymorpha*) also occur in this interval.

The Abu Roash F Member was represented by samples 15/349 and 15/387 (Supplementary data; Table 1). It was dominated by sheet-like, heterogenous masses of AOM, with a minor contribution of dinoflagellate cysts and microforaminiferal linings. Acritarchs (*Micrhystridium* sp.) and

Leiosphaeridia were infrequent (Fig. 7a, b). In addition, torn and poorly preserved sporomorphs (*Concavisporites* sp., *Retimonocolpites* sp., *Triplanosporites* sp.) were recorded along with poorly preserved phytoclasts (Fig. 7). Incident blue light fluorescence shows that the retrieved AOM particles (Fig. 7) could represent Type D amorphous kerogen (Thompson and Dembicki 1986).

A total of 7 samples from the E Member were investigated palynologically (Supplementary data; Table 1). They had low to moderate palynomorph yields and included a mixture of phytoclasts and AOM (Fig. 8). Phytoclasts were the main component in all samples, except for sample 15/339 which was dominated by AOM. Phytoclastic elements in this palynofacies assemblage were generally lath-shaped to equidimensional, brown-colored, and sometimes opaque. Biodegraded plant remains, cuticles, wood, and tracheids occurred frequently (Fig. 8). Algae were mainly represented by *Pediastrum* and *Botryococcus*. Spores included *Concavisporites* sp., *Triplanosporites* sp., and aquatic ferns such as *Ariadnaesporites*, *Crybelosporites pannuceus*, and *Gabonisoris* spp. Gymnosperm pollen were dominated by ephedroids (*Ephedripites*, *Equisetosporites*, *Steevesipollenites*) and *Araucariacites* sp. Angiosperm pollen comprised *Cretacaeiporitis polygonalis*, *Foveotricolpites gigantoreticulatus*, *Monocolpopollenites* sp., *Retitricolpites* sp., *Stellatopollis* sp., and *Tricolpites* spp. Marine elements encompassed dinoflagellates (*Cleistosphaeridium* sp., *Oligosphaeridium* sp., *Spiniferites* spp., and *Subtilisphaera* sp.) and microforaminiferal linings (Fig. 8).

Only sample 15/336 was available for palynological investigation of the D Member. It displayed a phytoclast-dominated assemblage with a minor contribution of AOM and palynomorphs (Fig. 9). Phytoclasts were generally yellow and brown, sometimes opaque, and included biodegraded wood, and cuticles. The palynomorphs were dominated by the colonial chlorococcalean alga *Pediastrum* sp. which showed variable degrees of preservation (Fig. 9), in addition to marine elements represented exclusively by microforaminiferal linings (Supplementary data; Table 2).

The C Member was represented by samples 15/327 and 15/328 which displayed moderately diverse and well-preserved palynomorphs. They comprised mainly non-marine lineages of algae (*Botryococcus* and *Pediastrum*) and spore taxa *Cyathidites australis*, *Cyathidites minor*, *Triplanosporites* spp., as well as aquatic ferns including *Crybelosporites pannuceus* and *Gabonisoris* sp. Pollen embraced *Cycadopites* sp., *Droseridites senonicus* (the most frequent element; Fig. 10e), *Ephedripites* spp., *Eucommiidites minor*, *Foveotricolpites giganteus*, *Retimonocolpites* spp., and *Tricolpites* spp. Marine elements were non-frequent and comprised dinoflagellate cysts (mainly *Cleistosphaeridium* spp. and *Cyclonephelium* spp.) and microforaminiferal linings (Fig. 10i, j). Palynofacies content constituted mixed

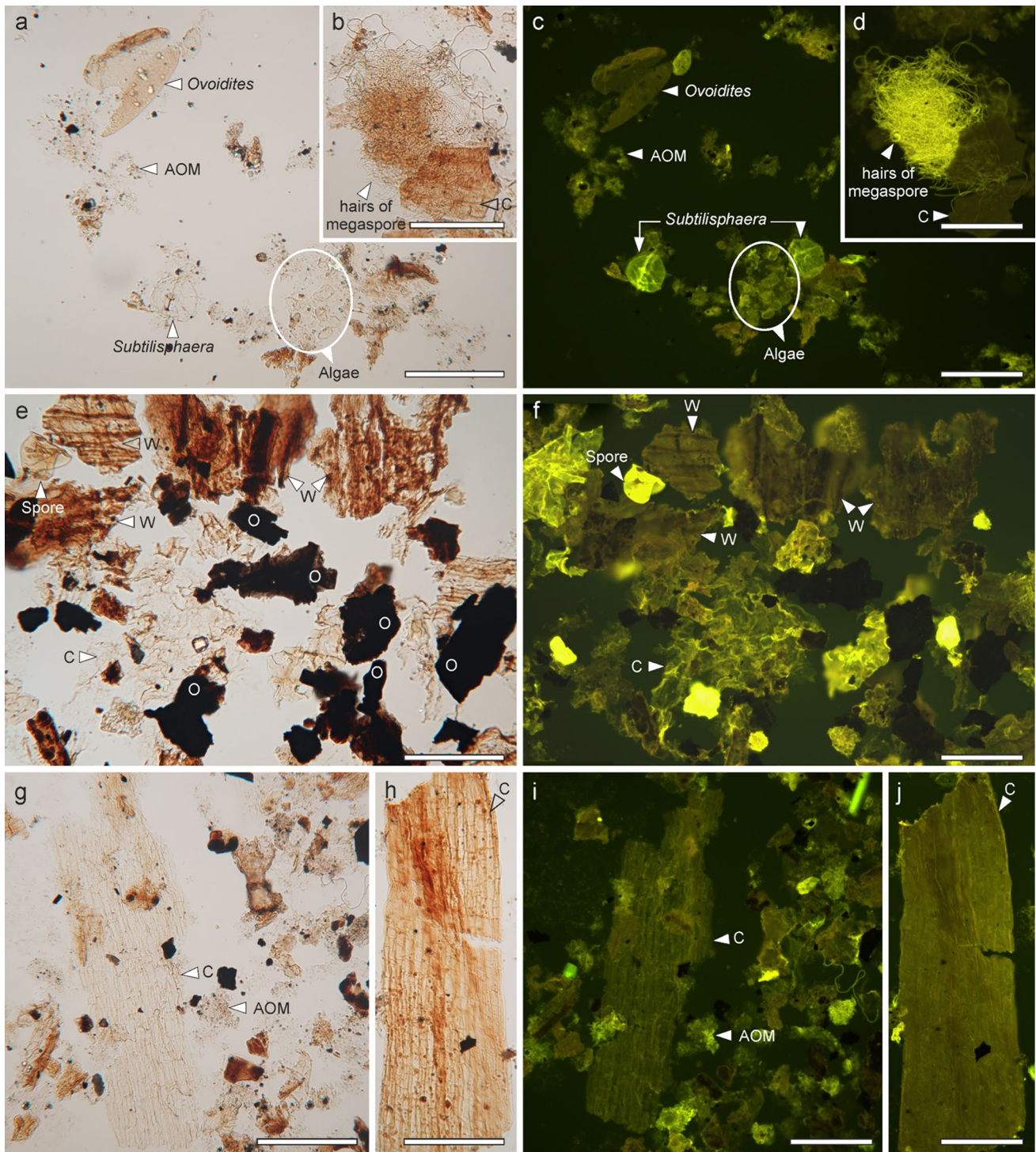


Fig. 6 OM assemblage characteristic for the Abu Roash G Member in the TSW-21 well, north Western Desert, Egypt as seen under transmitted white light and incident UV fluorescence microscopy. **a, c** Fluorescent AOM clots with ovoid zygospore or aplanospore of the Zygnemataceae (*Ovoidites*), algal clump and *Subtilisphaera* dinoflagellate cysts (arrows) (Sample 15/364). **b, d** Detached megaspore hairs seen distally coiled (arrow) and cuticles (C) (Sample 15/354).

e, f Palynofacies assemblage includes well-preserved non-fluorescent black and opaque specks (O) and brown-striped woody and tracheidal phytoclasts (W), fluorescent cuticle (C) tissues (Sample 15/391). **g–j** Well-preserved cuticles (C) present a clear cellular internal structure mixed with small fluorescent AOM masses (i, k: Sample 15/354; j, l: Sample 15/352). Scale bars: 100 µm

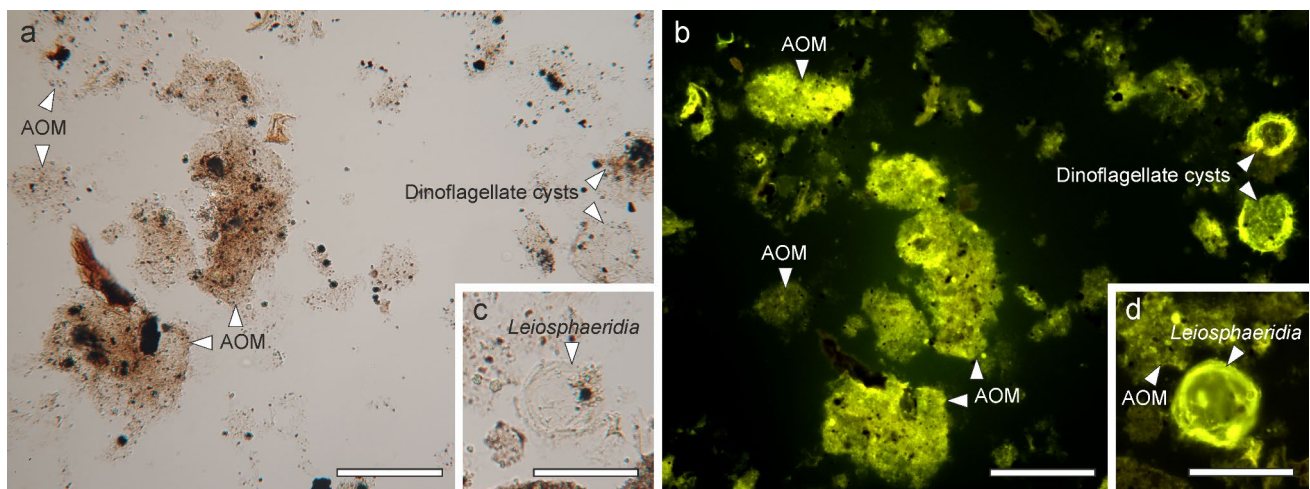


Fig. 7 OM assemblage characteristic for the Abu Roash F Member in the TSW-21 well, north Western Desert, Egypt as seen under transmitted white light and incident UV fluorescence microscopy. **a–d** Well-preserved AOM with specks (some of the specks are pyrite) presents a flaky shape, a lumpy or granular texture, diffuse outlines,

and variable size together with non-frequent dinoflagellate cysts and *Leiosphaeridia* assemblages. Note the strong fluorescence of AOM and the occurrence of unidentifiable fine fragments (Sample 15/349). Scale bars: 100 μm

assemblages of heterogenous, clotted, fine-grained, granular, pale AOM, and biodegraded phytoclasts. The latter group comprised mainly cuticles and wood with a minor opaque contribution (Fig. 4). Incident blue light fluorescence shows that the retrieved AOM particles could represent Type A and minor contribution of Type B amorphous kerogen (Thompson and Dembicki 1986).

The B Member could not be studied for palynology and palynofacies, but 7 samples were analyzed for organic geochemistry (Supplementary data; Table 1). Only sample 14/1348 represented the Abu Roash A Member. It was palynologically sparse (Fig. 11), except for *Ariadnaesporites* sp., a single record of *Droseridites senonicus*, a few torn dinoflagellate cysts, *Scenedesmus*, and microforaminiferal linings. Its palynofacies content was noticeably different from the preceding Abu Roash C Member. The A Member content was dominated by a heterogenous, clotted appearance, fine-grained, granular, pale AOM, and biodegraded phytoclasts that comprised cuticles and wood with a minor opaque contribution as seen under the transmitted white light microscope (Fig. 11). Incident blue light fluorescence showed that the retrieved AOM particles could represent a mixing of both Type A and D amorphous kerogen (Thompson and Dembicki 1986).

Organic petrography

Organic petrography was carried out on 12 samples from the Abu Roash C, E, F, and G members and the Bahariya Formation. Vitrinite reflectance was measured on 8 of the 12 samples, ranging from 0.45 to 0.60% R_o (Supplementary data;

Table 1). Apart from vitrinite, organic particles belonging to the maceral groups inertinite and liptinite were observed. Inertinite was present in relatively large quantities in all samples, whereas liptinite was less abundant. Furthermore, samples with high TOC contents are characterized by the presence of bitumen.

Samples of the Bahariya Formation contained mainly inertinite and vitrinite. OM was present mainly in the form of small, individual grains, making further differentiation of maceral subgroups difficult. Furthermore, intergranular bitumen occurred occasionally (Fig. 12a). Consistent with low TOC content, most of the samples examined microscopically from the Abu Roash G Member contained minor amounts of OM (liptinite, vitrinite, and inertinite; Fig. 12b). Bitumen was abundant in the upper stratum of the G Member (15/388) and it was present as dark elongated streaks with low reflectance and low/no fluorescence (Fig. 12c). The highest abundance of microscopically visible OM was observed in the F Member (15/551), with a high abundance of AOM, i.e., bituminite (Fig. 12d), and a minor occurrence of vitrinite and inertinite. The E Member contained vitrinite and inertinite particles. Occasional dark grain margins suggested the presence of bitumen. The carbonate-rich and organic-lean sample 15/326 of the Abu Roash C Member lacked organic particles.

Elemental analysis

The Bahariya Formation had an average TOC content of 2.01 wt% (range 0.27–6.02 wt% (Supplementary data; Table 1; Fig. 4). The formation was characterized by the

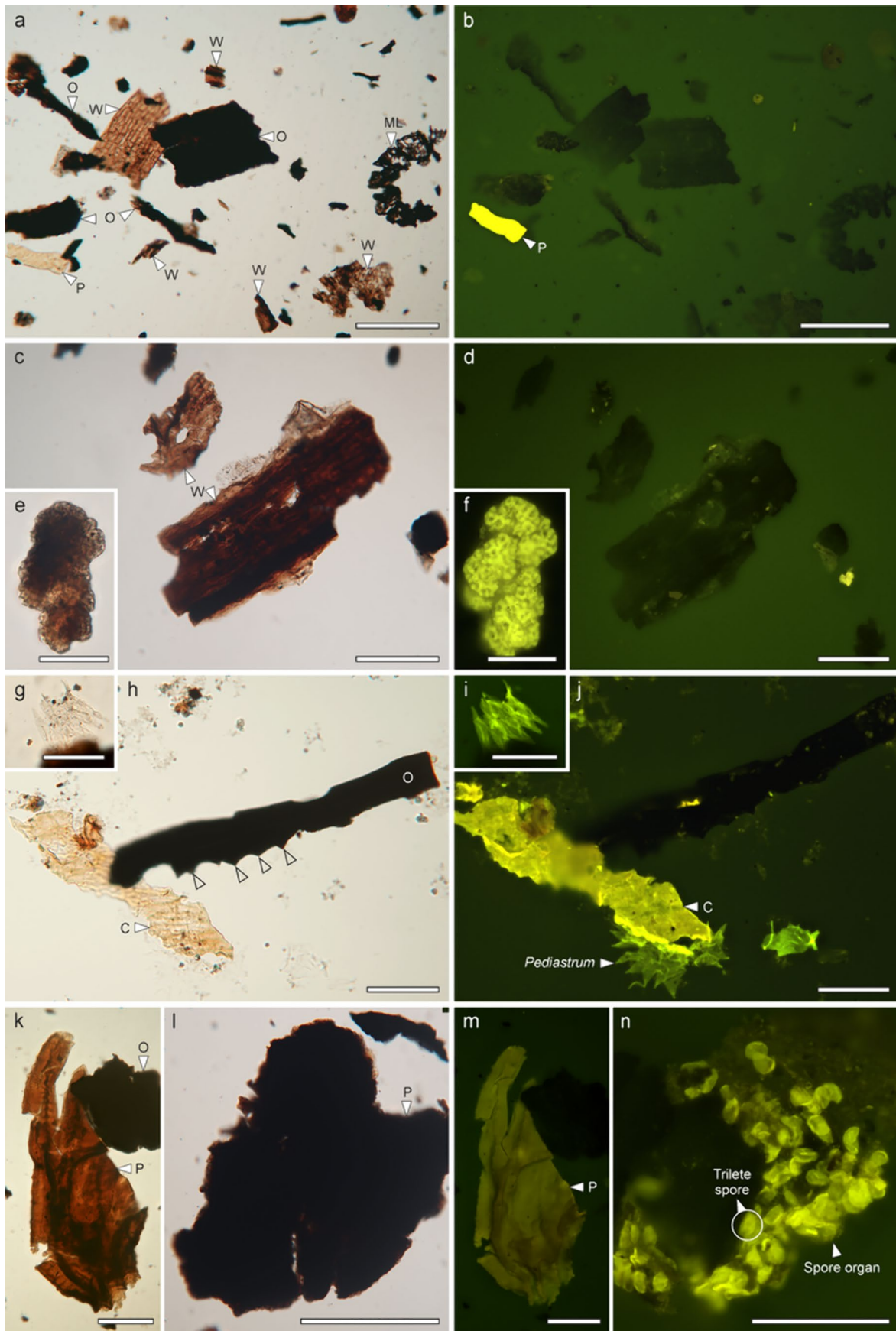


Fig. 8 OM assemblage characteristic for the Abu Roash E Member in the TSW-21 well, north Western Desert, Egypt as seen under transmitted white light and incident UV fluorescence microscopy. **a, b** A representative snapshot displaying a mixed association mainly of opaque phytoclasts (O), brown and brown-striped wood and tracheid debris (W), strongly fluorescent plant tissue (P) as well as non-fluorescent microforaminiferal lining (ML) (Sample 15/340) **c, d** Non-fluorescent lath-shaped brown wood particles (W) with horizontal and vertical elements and cross-field pitting as a typical component of this assemblage (Sample 15/337). **e, f** Well-preserved *Botryococcus* coenobia (Sample 15/338). **g, i** Well-preserved *Scenedesmus* coenobia (Sample 15/340). **h, j** Lath-shaped plant tissues including cuticles (C) as well as opaques (O) with possible residual botanical structures (arrows), in addition to highly fluorescent *Pediastrum* coenobia (Sample 15/343). **k, m** Fluorescent plant tissues (P) and non-fluorescent opaque particle (O) (Sample 15/340). **l, n** Dark-colored plant tissue (P) with a spore mass, probably part of a sporangium, UV fluorescence microscopy reveals numerous trilete spores (Sample 15/340). Scale bars: 100 μ m

lowest values for CaCO_3 (average 3.93 wt%; range 0.04–8.48 wt%). TS contents averaged 0.9 wt% with a range of 0.68–1.03 wt%.

While TOC and TS content for the Abu Roash G Member was similar to that for the underlying Bahariya Formation, averaging 1.54 wt% (range 0.4–2.78 wt%) and 0.7 wt% (0.13–1.32 wt%) respectively, the CaCO_3 content for the G Member was significantly higher, averaging 14.22 wt% and attaining 77.41 wt%. TOC values from the F Member reached 4.44 wt% (sample 15/341) and ranged from 0.20 to 4.44 wt%. This unit again included carbonate-rich and carbonate-poor samples, with highly variable CaCO_3 content (0.53–49.4 wt%). The TS content was increased at an average of 1.17 wt% (range 1.09–1.24 wt%). The Abu Roash E Member had an average TOC content of 1.96 wt% (range 1.23–4.42 wt%). The carbonate content was significantly higher in the upper part of the member (1743–1800 m) with an average of 28.11 wt% CaCO_3 , compared to the lower interval (1806–1845 m) which averaged 8.06%. Moreover, this unit was characterized by the highest sulfur content of all rock units in the TSW-21 profile, reaching 2.15 wt% (15/344), with an average value of 1.58 wt%. The TOC content for the D Member showed a decrease (average 1.09 wt%; range 0.66–2.08 wt%). In contrast, the CaCO_3 content was significantly higher (average 58.44 wt%; range 26.14–80.82 wt%). The total sulfur content was 1.48 wt%. The C Member had an average TOC content of 1.23 wt% (0.68–1.83 wt%). The CaCO_3 content was low at the base of the unit (minimum 12 wt%) and increased towards the top (reaching 70.7%). The sulfur content on sample 15/328 was measured at 1.89 wt%. The Abu Roash B Member had the lowest average TOC content (0.79 wt%; range 0.55–1.02 wt%) and the highest carbonate content at 81.44% (average 61.89%). The sulfur content was relatively low at 0.83 wt% for sample 15/323. The TOC content in the uppermost A Member

averaged 1.14 wt% and varied between 0.93 and 1.54 wt%. The carbonate content was high (57.98% on average), ranging from 26.45 wt% CaCO_3 at the base to 72.29% at the top of the unit. The TS content was 1.48 wt% for sample 15/316.

Rock–Eval pyrolysis

HI values were relatively low in the well section TSW-21, with an average of 62 mg HC/g TOC and values below 300 mg HC/g TOC for all samples, except for one sample (15/351) in the Abu Roash F Member, where HI reached 592 mg HC/g TOC (Fig. 13). The OI showed a decrease with depth, with the highest values observed in upper Abu Roash Members A and B (averaging 145 and 143 mg CO_2 /g TOC respectively), and the lowest in the Bahariya Formation (average 33 mg CO_2 /g TOC). The calculated PI of the samples ranged from 0.08 (Abu Roash E, G, and Bahariya) to 0.52 (Bahariya) (Supplementary data; Table 1; Fig. 4).

The Bahariya Formation was characterized by relatively low or moderate HI values (range 118–199 mg HC/g TOC overall), but with elevated HI readings from 2041 to 2051 m (reaching 349 mg HC/g TOC). In addition, average OI values in this unit are the lowest for the sampled borehole, reaching a minimum of 19 mg CO_2 /g TOC (sample 15/398).

The Abu Roash G Member HI was highly variable, ranging from 71 to 356 mg HC/g TOC (average 152 mg HC/g TOC). The average OI was 47 mg CO_2 /g TOC (range 14–67 mg CO_2 /g TOC). The F Member was characterized by the highest HI values, with a maximum of 592 mg HC/g TOC (sample 15/351). HI values varied widely in this unit, featuring a minimum value of 92 mg HC/g TOC. The average OI in this interval was 53 mg CO_2 /g TOC. Member F also had the lowest PI values in the well section, with an average of 0.13. The HI of the E Member samples ranged from 100 to 359 mg HC/g TOC (average 173 mg HC/g TOC). The OI was sustained with an average value of 50 mg CO_2 /g TOC. The Abu Roash D Member displayed a reduced HI overall (average of 140 mg HC/g TOC). The OI was higher at an average of 87 mg CO_2 /g TOC than for underlying units, with values increasing towards the top of the studied section. The C Member had an average HI of 124 mg HC/g TOC (range 90–156 mg HC/g TOC) and an average OI of 77 mg CO_2 /g TOC (range 63–93 mg CO_2 /g TOC). The HI of Abu Roash B remained consistent (average 159 mg HC/g TOC; range 117–211 mg HC/g TOC) with the levels in the underlying rock units, though the OI increased (average 143 mg CO_2 /g TOC), with the highest reading of 195 mg CO_2 /g TOC in sample 15/231. At the top of the well section, the A Member was characterized by average HI value (129 mg HC/g TOC) and OI values (averaging 145 mg CO_2 /g TOC).

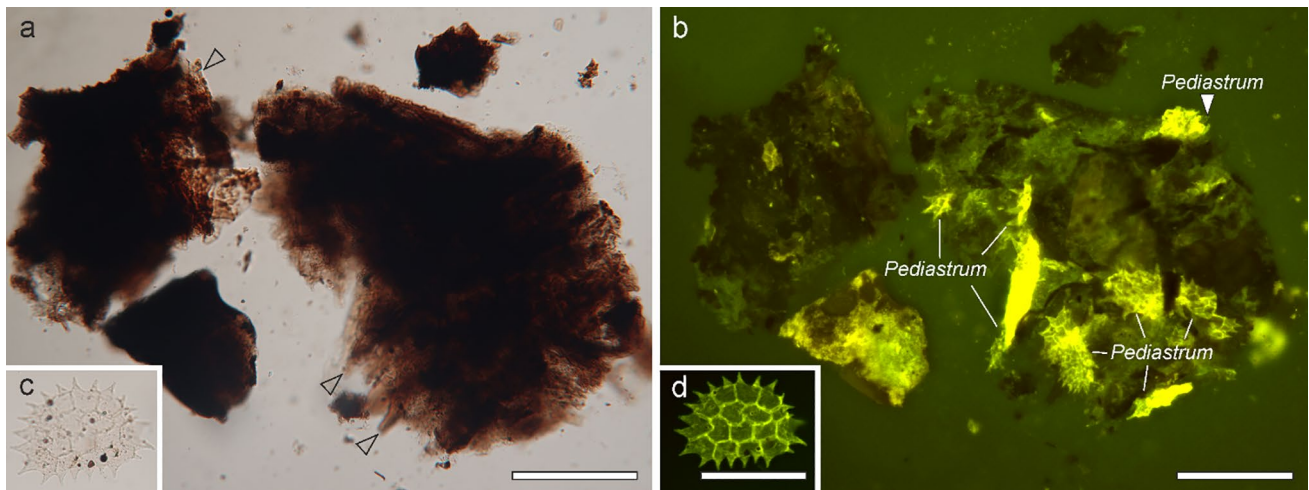


Fig. 9 Typical OM assemblage characteristic for the Abu Roash D Member (sample 15/336) in the TSW-21 well, north Western Desert, Egypt as seen under transmitted white light and incident UV fluorescence microscopy. **a** Massive phytoclast particles with distinct edges (arrows) and no clear internal structures. **b** Incident UV fluorescence shows non-fluorescent phytoclasts mixed with fluorescent phytoclast

particles and moderately preserved *Pediastrum* specimens that are undetected under the transmitted white light microscope (Sample 15/336). These massive phytoclasts typically represent lignites, coals, and terrestrial OM-rich sediments (Tyson 1995), as supported also by high TOC readings. **c**, **d** Well-preserved *Pediastrum* coenobium (Sample 15/336). Scale bars: 100 μm

Biomarker distribution

Three of the 13 samples examined for molecular geochemical composition showed Pr/Ph ratios above 1 belonging to both the Bahariya Formation and Abu Roash E and G members. The remaining samples had Pr/Ph values below 1, of which 5 samples were less than 0.9 (Bahariya, Abu Roash G, B, and A) (Supplementary data; Table 3; Fig. 4).

The ratios of acyclic isoprenoids to *n*-alkanes reached their minimum and maximum in the Bahariya Formation, ranging from 0.42 (Pr/*n*C17) and 0.32 (Ph/*n*C18) to 2.34 (Pr/*n*C17) and 2.81 (Ph/*n*C18), respectively. In the Abu Roash Formation, the ratios ranged from 0.41 to 1.35 (Pr/*n*C17) and 0.37 to 1.22 (Ph/*n*C18), with a minimum in the Abu Roash D Member (15/336) and a maximum in the E Member (15/341) (Supplementary data; Table 3; Fig. 14).

The TAR was low in 10 of the 13 samples examined, with a maximum of 0.29. TAR values above 2 were observed in the Abu Roash G Member and the Bahariya Formation, reaching a maximum of 8.51 in the upper Bahariya Formation (15/395). CPI values close to 1 indicate a balanced distribution of odd- and even-numbered *n*-alkanes. The minimum CPI recorded in the Abu Roash E Member (15/341) was 0.87, and the maximum value was observed in the Bahariya Formation (15/370) with 1.3 (Supplementary data; Table 3).

A clear dominance of hopanes over steranes was observed in 12 of the 13 samples as indicated by sterane/

hopane ratios of ≤ 0.5 . A dominant abundance of steranes over hopanes (steranes/hopanes = 1.61) was found exclusively in the sample 15/351 from the Abu Roash F Member (Supplementary data; Table 3).

While C_{27} Ts/(Ts + Tm) ratios were relatively low, varying between 0.08 (Abu Roash E) and 0.36 (Abu Roash A), the isomerization ratio C_{31} Hop 22S/(22S + 22R) was high, ranging from 0.44 to 0.58, indicating that isomerization equilibrium had probably been achieved. The moretane/hopane ratio ranged between 0.12 (Abu Roash A and G) and 0.40 (Abu Roash E). The GI was generally low and reached its maximum in the Abu Roash F Member with a value of 2.04 (Supplementary data; Table 3).

The C_{27} diasterane/sterane ratio ranged from 0.02 (Abu Roash E) to 0.2 (Abu Roash C). The ratio of the regular C_{29} 20S and 20R sterane isomers, at 0.32–0.51, suggested that equilibrium had not been achieved. The relative abundances of regular steranes ($\alpha\alpha\alpha$ R) ranged from 7 to 41% for C_{27} , 25 to 67% for C_{28} , and 19 to 46% for C_{29} . Five samples from the Abu Roash A, B, D, and E members were characterized by strikingly high C_{28} regular sterane concentrations with relative concentrations reaching up to 67%. They were accompanied by particularly low C_{27} regular sterane relative concentrations at a minimum of 7%. High C_{28} ranges were additionally indicated by high C_{28}/C_{29} ratios above 2.6 (Supplementary data; Table 3).

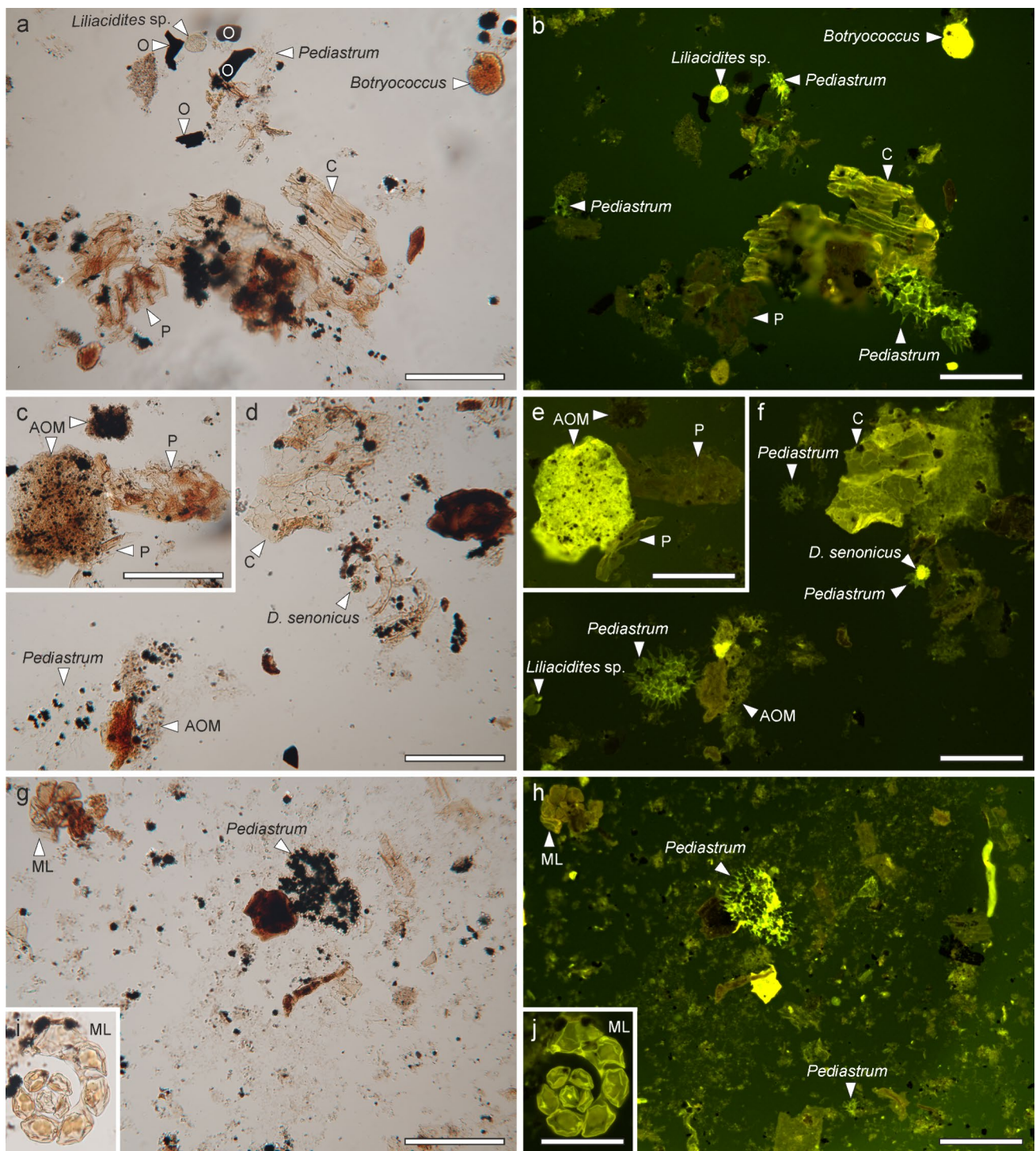


Fig. 10 OM assemblage characteristic for the Abu Roash C Member in the TSW-21 well, north Western Desert, Egypt as seen under transmitted white light and incident UV fluorescence microscopy. **a, b** Mixed palynofacies assemblages dominated by cuticles (C) as well as non-fluorescent plant tissues (P) and opaque phytoclasts (O) in addition to algae of *Pediastrum* and *Botryococcus* with *Liliacidites* pollen grain which is diagnostic for this time interval (see also **f**) (Sample 15/328). **c, e** Well-preserved and densely specked highly fluorescent AOM together with non-fluorescent AOM, and phytoclast particles

including plant tissues (P) (Sample 15/327). **d, f** Mixed palynofacies assemblages composed of cuticles (C) as well as fluorescent AOM in addition to frequent *Pediastrum* coenobia and the age-diagnostic pollen taxa of *D. senonicus* and *Liliacidites* sp. (Sample 15/328). **g-j** Note the difference in the color of both coiled microforaminiferal linings (ML) which is also reflected in fluorescence and also the high pyrite input which obliterates the cellular structure of *Pediastrum* coenobium (clearly seen in **g**) (Sample 15/327). Scale bars: 100 μ m

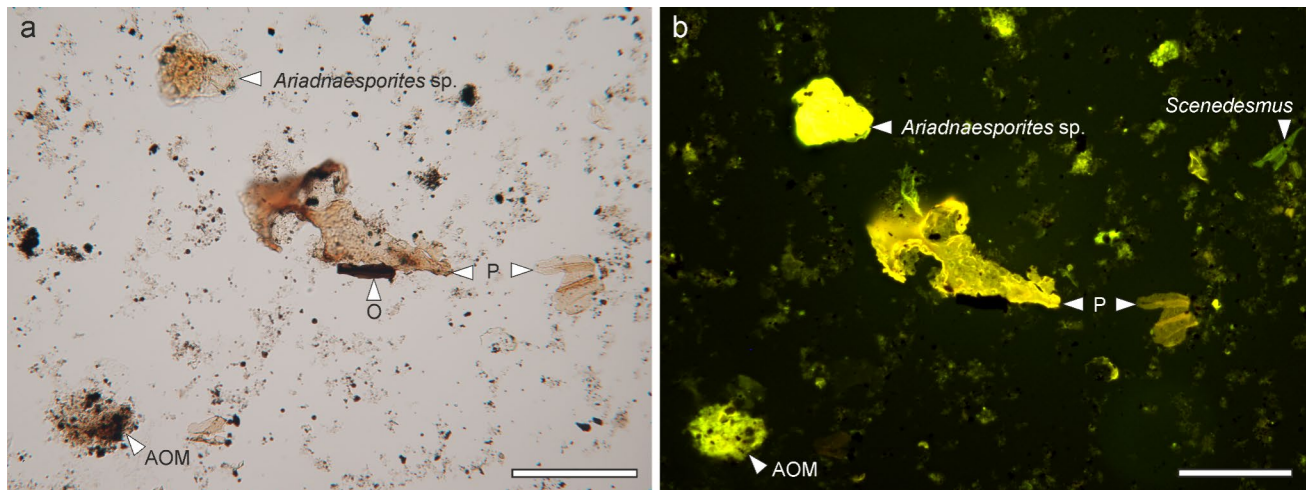


Fig. 11 Typical OM assemblage characteristic for the Abu Roash A Member in the TSW-21 well, north Western Desert, Egypt as seen under transmitted white light and incident UV fluorescence microscopy. **a** Poorly preserved palynofacies assemblage dominated by fine-

grained AOM and biodegraded phytoclasts including plant tissues (P) and opaques (O), rare palynomorphs are recognizable. **b** Fluorescent AOM and phytoclast particles as well as broken *Scenedesmus* cells (Sample 14/1348). Scale bars: 100 µm

Discussion and interpretation

Botanical aspects and vegetation

Fern spores, including aquatic forms, were frequent in the palynological assemblages, whereas pollen and fungal spores as well as freshwater elements (*Botryococcus*, *Pediastrum*) were less well represented, throughout the borehole record except for some intervals (Supplementary data; Table 2). Marine entities (dinoflagellate cysts, acritarchs, and microforaminiferal linings) were also dominant in the Bahariya and Abu Roash formations (Supplementary data; Table 2). Sporomorphs were grouped into four plant categories to facilitate the interpretation of floristic composition: spores, gnetalean gymnosperm pollen, non-gnetalean gymnosperm pollen, and angiosperm pollen (cf. El Atfy et al. 2023b). Palynologically, vegetation types documented by the palynoflora are based on comparisons between the botanical affinities of fossil taxa and the closest modern analogs.

Fern spores (e.g., Fig. 6e, f) belonging to the Matoniaceae were distinctive elements (*Concavisporites*, *Trilobosporites*, *Matonisporites*). Other ferns were chiefly affiliated with Filicopsida: Cyatheaceae (*Cyathidites*), Lygodiaceae (*Triplanosporites*), and Selaginellaceae (*Leptolepidites psarosus*). In addition, riparian and freshwater wetland communities favoring aquatic and/or hygrophilous ferns (Salviniaceae and Marsileaceae) of the taxa *Ariadnaesporites* (Fig. 11), *Crybelosporites*, and *Gabonisoris* were also noted (e.g., Balme 1995). The significance of Salviniaceae in the fossil record as an indicator of relatively warm, still, freshwater paleoenvironments has long been recognized (Vajda and McLoughlin 2005). Their co-existence with freshwater algae

implies fresh open water, or a lacustrine environment (e.g., Vallati et al. 2017; El Atfy et al. 2023c).

Non-gnetalean gymnosperm pollen encompassed Cycadales, Ginkgoales, and Bennettitales (*Exesipollenites*) along with conifers incorporating Araucariaceae (*Araucariacites* and *Balmeiopsis*) and Cheirolepidiaceae (*Clasopollis*). In contrast, gnetalean elements were represented exclusively by ephedroids (*Ephedripites*, *Equisetosporites*, *Steevesipollenites*). Angiosperm pollen formed the most diverse component within the sporomorph group (Supplementary data; Table 2).

Depositional environment

Generally, variation in depositional environments, especially short-term changes, has a significant impact on the parent vegetation and resultant sporomorph and organic particle assemblages. It may also have an impact on the differential preservation of specific taxa due to taphonomic processes (Slater and Wellman 2016). In general terms, the floristic configuration of the Upper Cretaceous succession, and especially the uppermost Abu Roash members (Supplementary data; Table 2), reflects mixed vegetation under the influence of short-term marine incursions. This is evidenced by the repeated occurrences of dinoflagellate cysts (e.g., Fig. 7c, d), microforaminiferal linings (e.g., Fig. 10i, g), and acritarchs. This mosaic vegetation could represent a range of depositional environments. In terms of paleoclimate, a warm and humid climate interrupted by dry phases might be deduced (e.g., El Atfy et al. 2023b).

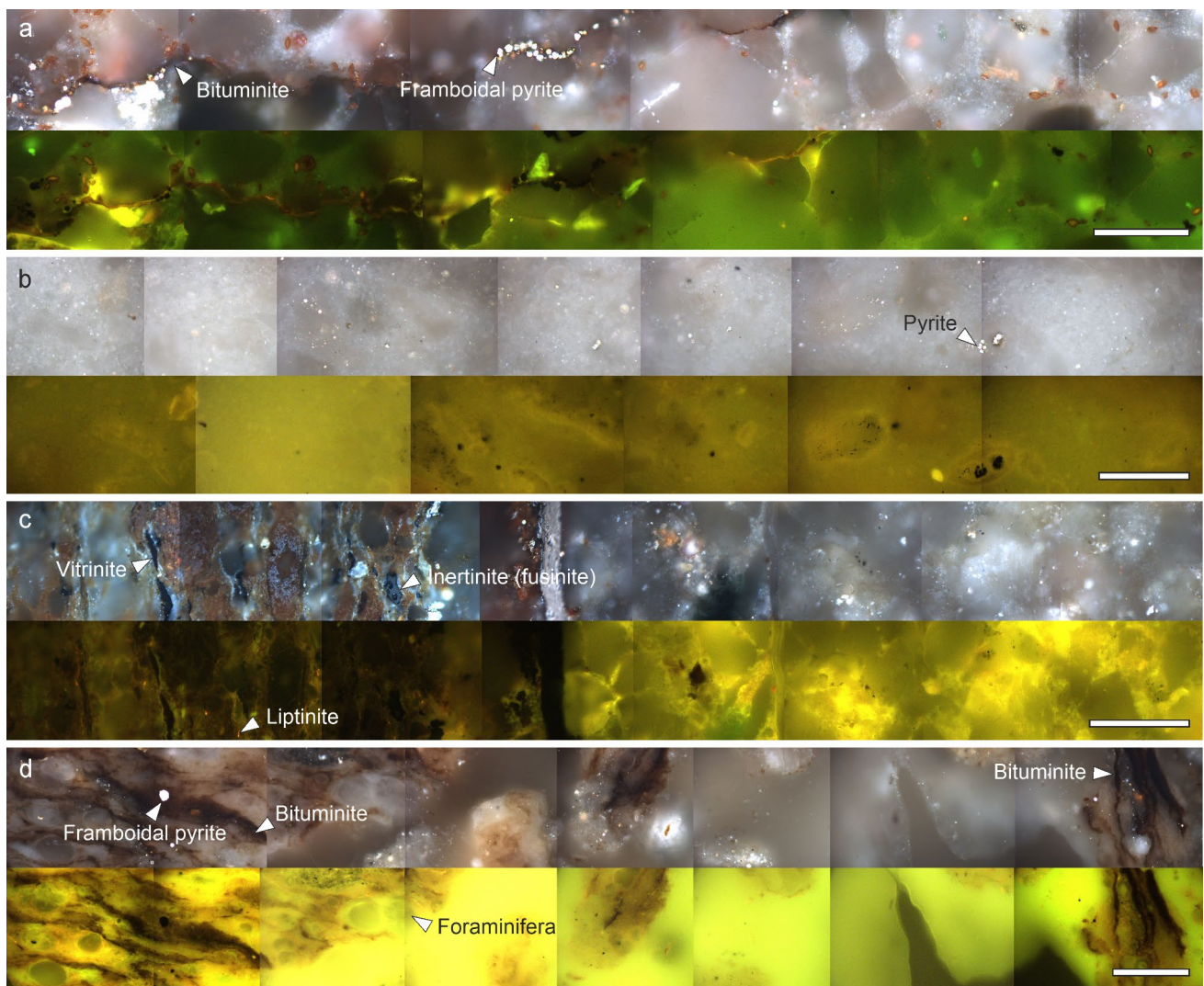


Fig. 12 Mosaics of microscopic images with labeling of observed features under reflected white light and UV light. **a** Sample 15/399 (Bahariya Formation). **b** Sample 15/393 (Abu Roash G). **c** Sample

15/388 (Abu Roash G). **d** Sample 15/351 (Abu Roash F), TSW-21 well, Western Desert, Egypt. Scale bars: 100 μ m

The basal section features the deposition of the Bahariya Formation which was known to have formed in a shallow marine regressive sea under fluvio-deltaic or shallow inner shelf conditions (0–50 m water depth) (Abdel-Kireem et al. 1996). This has been confirmed by palynofacies results (e.g., El Beialy et al. 2010a; Ghassal et al. 2018). The palynofloras from the current study are dominated by terrestrial elements such as fern spores, gymnosperm and angiosperm pollen, and a few marine palynomorphs. This low diversity sporomorph assemblage suggests that deposition could have taken place in the vicinity of a shoreline. Furthermore, the persistent occurrence of freshwater aquatic fern spores reveals the existence of swamps or water-logged environments (Batten et al. 1994). The general aspect of the palynological assemblages is consistent with accumulation in a shallow

shelf environment (cf. macrofloral evidence in El Atfy et al. 2023b). The associated organic detritus is predominantly composed of inertinite and vitrinite, suggesting high inputs of terrigenous OM. Overall, deposition in a shallow, near-shore environment close to well-vegetated terrestrial areas is indicated.

Marine elements are dominated by the dinoflagellate taxa *Circulodinium*, *Coronifera*, *Cyclonephelium*, *Oligosphaeridium*, *Spiniferites*, and *Subtilisphaera*. Together with microforaminiferal test linings, the dinoflagellate cysts suggest deposition in a coastal or shallow marine environment of normal salinity (Mahmoud et al. 2007; El Atfy 2021). It is also important to highlight the *Subtilisphaera* blooming (e.g., Fig. 5f) near the top of the Bahariya Formation and towards the lower part of the

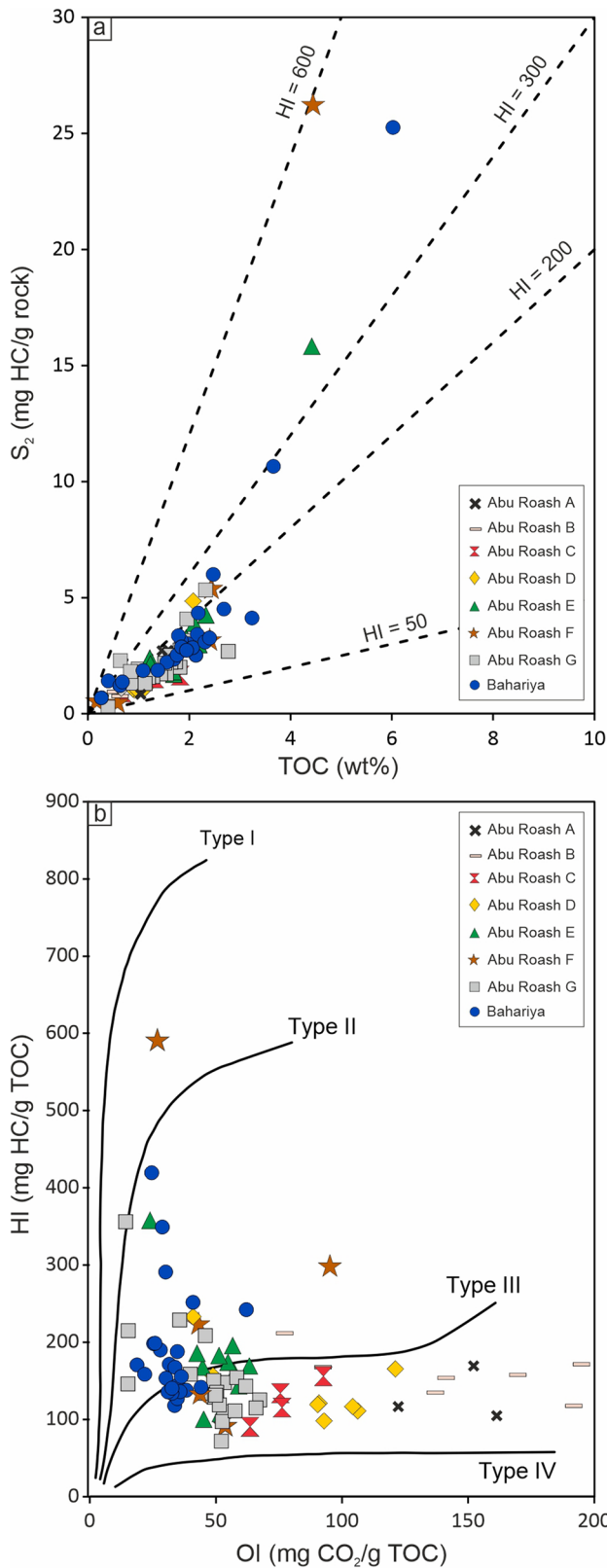


Fig. 13 a TOC versus Rock-Eval S_2 of source rock samples. b Pseudo-van Krevelen diagram of HI versus OI of source rock samples, TSW-21 well, Western Desert, Egypt

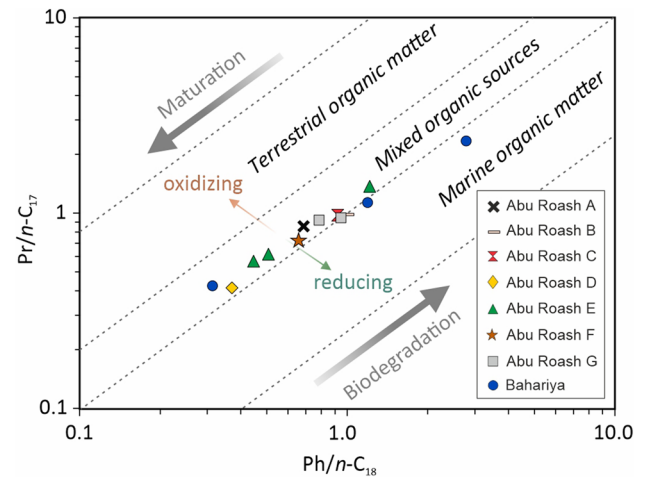


Fig. 14 Cross-plot of Pr/nC_{17} versus Ph/nC_{18} (Shanmugam 1985), indicative of paleodepositional setting, redox potential, and thermal maturation, TSW-21 well, Western Desert, Egypt

Abu Roash G Member. Such an ecological datum has been identified previously from the North Western Desert (Ibrahim et al. 2009) and Sinai (El Beialy et al. 2010b). This was interpreted by El Beialy et al. (2010b) as an extension to the mid-Cretaceous *Subtilisphaera* ecozone (e.g., Arai et al. 2000), implying a near-shore low-latitude environment. This finding is confirmed by the minor presence of liptinite, the correlation of Pr/nC_{17} versus Ph/nC_{18} , and

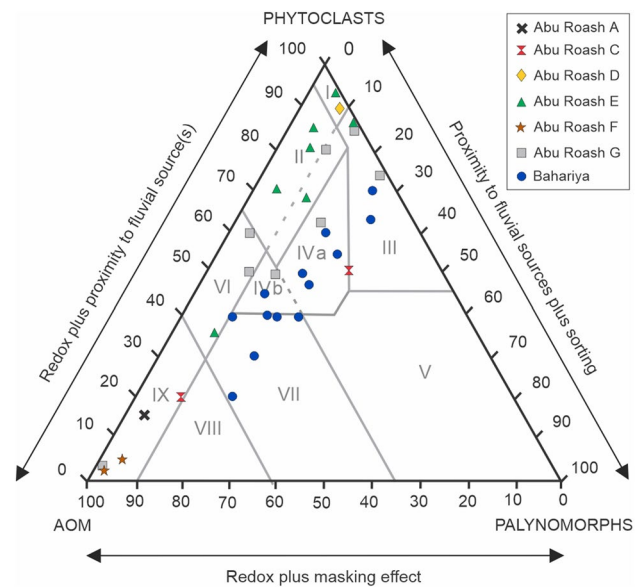


Fig. 15 APP ternary diagram (Tyson 1989) of the studied samples from the TSW-21 well, Western Desert, Egypt; field I=kerogen Type III, field II=kerogen Type III, field III=kerogen Type III or IV, field IV=kerogen Type III or II, field V=kerogen Type III>IV, field VI=kerogen Type II, field VII=kerogen Type II, field VIII=kerogen Type II>I, field IX=kerogen Type II>I. For the assignment of palynofacies fields to environments, see Tyson (1995; Table 25.2)

the distribution of C_{27} – C_{28} – C_{29} regular steranes (Peters et al. 2005).

In addition, palynofacies data indicated that the Bahariya Formation was deposited in a proximal suboxic to oxic shallow marine to fluvio-deltaic environment, where high terrestrial/freshwater inputs were mixed with marine organic matter. This is illustrated by the AOM-phytoclast-palynomorph (APP) ternary diagram of Tyson (1989), which revealed that the Bahariya samples are located mainly within fields VII and IV, with only two samples in field III (Fig. 15). Field VII implies distal dysoxic-anoxic deposition. In contrast, fields IV and III refer to proximal shelf depositional settings. This is further supported by the relatively high Pr/Ph ratio and Pr/n- C_{17} and Ph/n- C_{18} .

The overlying Abu Roash Formation shows similar palynomorph assemblages, especially within the basal G Member (Fig. 6). However, up-profile increases in marine elements and AOM (Fig. 4) imply a transgressive phase. Marine transgression reaches its highest reflection in the F Member, corresponding to the Cenomanian–Turonian oceanic anoxic event (OAE2; e.g., Ghassal et al. 2018). The event is also seen in the high abundance of marine AOM and lack of vitrinite in the organic petrology results, high steranes over hopanes indicating high marine algal inputs, and high HI from Rock–Eval pyrolysis, denoting high OM preservation. Although dinoflagellate cysts and microforaminiferal linings are well preserved and imply deposition in a marine environment (e.g., Fig. 7c, d), the occurrence of terrestrial inputs is usually taken to indicate relative proximity to shorelines. The latter is strongly suggested by the occurrence of lath-shaped phytoclasts and other plant debris, including sporangia (e.g., Fig. 8n), in addition to terrestrial palynomorphs (e.g., Fig. 10a, b). Algal coenobia expand, mainly *Pediastrum* and *Botryococcus*, with a minor contribution of *Scenedesmus* (Figs. 9, 10). These are key elements, especially in the Abu Roash E and D members. Such an ecological datum, as assigned to a chlorococcalean green alga interregnum (Schrank and Ibrahim 1995) later highlighted by many others (e.g., El Atfy et al. 2017), is taken as clear evidence of terrestrial inputs. The biomarker data from the Abu Roash samples, based on the Pr/n- C_{17} and Ph/n- C_{18} correlations (Fig. 14), also indicate diverse marine and terrestrial contributions.

The APP ternary plot diagram of Tyson (1989) revealed that Abu Roash G samples were located mainly within fields VI and IV, with two samples in field III; all consistent with deposition in a proximal shelf environment (Fig. 15). The samples from the F Member, which generally yielded AOM with a lower abundance of palynomorphs, were located within the IX field, signifying that deposition may have taken place in a distal suboxic-anoxic basin. The E Member samples, located within fields VI, III, II and I, suggest marginal and proximal deposition. A single sample only is

available from the D Member and it plots within field I, reflecting a highly proximal setting for deposition. The C Member is represented by 2 samples located in a shelf-to-basin transition (field IVa) and a distal suboxic–anoxic basin (field IX). The same inference applies for the uppermost part of the Abu Roash A Member. The interplay between marine and non-marine influences is reflected in TAR ratios that indicated regressive phases dominated by terrestrial inputs in all rock units other than for the Abu Roash F Member. The latter witnessed transgressive phases during the OAE2 period. The distribution of inertinite and vitrinite versus liptinite and AOM proportions in the petrographic analyses showed a general abundance in terrestrial OM input (excluding the F Member).

The abundance of AOM, mostly of terrestrial origin, and the presence of framboidal pyrite in some intervals of the Abu Roash (and Bahariya) formations, suggest the restricted circulation of low-density water in a middle to outer shelf environment as reported from the IVA zone (Vraconian to early Cenomanian) of northeast Libya (Uwins and Batten 1988). Such a finding was recognized in palynological macerals and also in the petrographic analysis (Fig. 12).

It may be concluded that data gained from palynology is supported by organic petrology and biomarker analyses. Apart from the Abu Roash F Member which is dominated by marine AOM and liptinite, all other rock units are dominated by inertinite and vitrinite with minor liptinite. This indicates a shallow proximal marine environment (e.g., Ghassal et al. 2018). Similarly, the general dominance of hopanes over steranes (excluding the F Member) also supports the palynological and organic petrological inferences.

Source rock potential

The integration of optical and geochemical methods is one of the best ways to investigate kerogen composition and to screen hydrocarbon source rock potential. In addition, palynology, organic petrology, and organic geochemistry are powerful tools for reconstructing paleoenvironmental settings (El Atfy et al. 2023a). In the current work, this integrated approach produces direct and robust evidence which greatly assists the interpretation of source rock potential for kerogen typing and thermal maturity investigation.

OM richness

OM richness is commonly determined by the TOC content and Rock–Eval S_1 , S_2 , and S_3 (Ghassal et al. 2023). Numerous empirical studies on samples from different locations

define TOC values for assessing the source rock potential (e.g., Peters 1986; Javier 1991; Hunt 1996). The factors that control the richness and preservation of organic matter are summarized by Ghassal and El Atfy (2023). Note that TOC indicates the overall OM richness, meaning it accounts for both the reactive and non-reactive (inert) organic matter. Therefore, S_2 , from Rock–Eval, is required to assess the source rock richness and the remaining potential.

The TOC content of the studied samples ranges from 0.27 to 3.67 wt% in the Bahariya Formation (Supplementary data; Table 1), revealing very good OM richness and source rock potential. The S_2 varies from 1.8 to 10.7 mg HC/g rock, indicating good to excellent remaining potential. For the overlying Abu Roash Formation, the TOC content ranges from 0.55 to 2.33 wt%, revealing fair to very good petroleum potential, except for a reading of 4.42 wt% for E Member sample 15/341, which displays excellent potential. In this well, the Bahariya and Abu Roash formations exhibited overall good source rock richness compared to other wells in the Abu Gharadig Basin (e.g., Ghassal et al. 2018; Elhossainy et al. 2022).

Kerogen type (quality)

Palynologically, the kerogen composition of each of the studied rock units reflects a variable mixture of two major OM contributors, phytoclasts and AOM, in addition to palynomorphs. Within the Bahariya Formation, the recorded AOM implies primarily gas-prone kerogen. The phytoclasts comprise remains of terrestrial macrophytes such as wood fragments, cuticles, cortex tissues, and oxidized plant particles (opaques). They make up the bulk composition of kerogen types III and IV. The APP ternary kerogen diagram shows that the Bahariya samples are located mainly within fields VII, IV, and only 2 samples in field III (Fig. 15). Field VII infers a Type II kerogen (oil-prone), field IV implies kerogen Type III or II (mainly gas-prone), whereas field III infers III or IV gas-prone kerogen types. The Bahariya Formation exhibited moderate HI and OI values (Supplementary data; Table 1; Fig. 13b), which imply that the source rock is oil- and gas-prone. The dominance of vitrinite and inertinite with minor liptinite has been identified in the organic petrology investigation. The identified AOM from the Abu Roash Formation refers mainly to AOM types A and D of Thompson and Dembicki (1986), indicating highly oil-prone kerogen. High AOM concentrations denote the presence of a kerogen Type I or II (Tyson 1995). The APP plot (field IX) supports this kerogen typing for the Abu Roash F, C, and A members – i.e., Type II > I kerogen. Samples from the G, E, and D members are also typical of gas-prone fields I, II, III, and IV. The geochemical analysis of the Abu Roash samples indicated mixed oil and gas petroleum potential of viable

quality. As supported by the highest HI value (Fig. 13b), the best quality was observed in an F Member sample.

Thermal maturity

An optical examination of spores and pollen exine in transmitted white light microscopy was employed to estimate the thermal maturity of palynomorphs. Maturity data followed Hartkopf-Fröder et al. (2015), the exine colors of Pearson (1984), and Spore Color Index (SCI) numbers and vitrinite reflectance after Marshall and Yule (1999), corresponding to the numerical scale of Thermal Alteration Index (TAI) according to Staplin (1969). The color of palynomorph exines from the Bahariya Formation varied between pale and medium yellow (SCI 2–3), (TAI 1+ to 2–), corresponding to a vitrinite reflectance of 0.3 to 0.5% R_o , suggesting immature OM. Palynomorphs recovered from the Abu Roash Formation display a pale to dark yellow color (SCI 2–4; TAI 1+ to 2) (e.g., Fig. 6e), equivalent to 0.3 to 0.5% R_o , indicating immature OM. This is consistent with the maturity assessment based on the average T_{max} of 431 °C, corresponding to 0.60% R_o (Evenick 2021), and the measured vitrinite reflectance, which varied from 0.47 to 0.60% R_o and 0.47 to 0.64% R_o for the Bahariya and Abu Roash samples, respectively (Supplementary data; Table 1).

Conclusions

Sensible source rock characterization requires meticulous investigation via integrated approaches, especially in under-explored basins. The integration of optical (i.e., palynology and organic petrography) and geochemical (i.e., elemental analysis, Rock–Eval pyrolysis, and molecular organic geochemistry) proxies allows a deep understanding of the factors controlling a source rock's organic richness, quality, and thermal maturity, providing robust inputs for basin and stratigraphic modeling. In the current study, cores and cuttings from the TSW-21 well were examined using a multidisciplinary and high-resolution approach, aimed at establishing a fingerprint for OM deposition in each rock unit studied, with the conclusions as follows:

1. The palynological analysis identified near-shore, marginal marine conditions for the middle Cretaceous Bahariya Formation. The infrequent occurrence of more diverse assemblages suggested occasional open-marine shelf sea environments for strata in the overlying Upper Cretaceous Abu Roash Formation. Similar conclusions were drawn from organic petrography and geochemical proxies.
2. TOC content ranged from 0.27 to 3.67 wt% in the Bahariya Formation, revealing good OM richness and source

rock potential. The S_2 varied from 1.8 to 10.7 mg HC/g rock, indicating good to excellent remaining potential. In the Abu Roash Formation, the TOC content ranged from 0.55 to 2.33 wt%, revealing fair to very good petroleum potential, except for one reading of 4.42 wt% in the E Member (sample 15/341), which displayed excellent potential.

3. In terms of kerogen type and OM quality, samples of the Bahariya Formation yielded the largest quantities of phytoclasts. AOM was generally sparse and probably derived mainly from land plants. Dinoflagellate cysts were abundant, morphologically diverse, and well preserved, implying deposition in a marine environment. The Bahariya Formation was dominated by mixed Type II, III or II and III or IV kerogen (high phytoclast and AOM), with gas-prone OM. On the other hand, the succeeding Abu Roash Formation contained Type II and I kerogen (AOM-rich), indicative of highly oil-prone OM.
4. Thermal maturity proxies encompassing T_{max} , $R_o\%$, and SCI generally indicated that both the Bahariya and Abu Roash formations were immature. The color of palynomorph exines from the Bahariya Formation varied between pale and medium yellow (SCI 2–3), corresponding to 0.3 to 0.5% R_o . Similarly, palynomorphs recovered from the Abu Roash Formation displayed a pale to dark yellow color (SCI 2–4), equivalent to 0.3 to 0.5% R_o . This is highly consistent with the average T_{max} reading of 431 °C.

Supplementary Information The online version contains supplementary material available at <https://doi.org/10.1007/s00531-024-02451-5>.

Acknowledgements The authors are grateful to the Egyptian General Petroleum Corporation (EGPC) and the General Petroleum Company (GPC) for providing samples and well logs for this study. We are grateful to two anonymous reviewers and to Ulrich Riller (Editor-in-Chief) for their detailed and helpful comments. We also extend our thanks to guest-editors Christoph Hartkopf-Fröder, Jan Schwarzbauer, and Peter Kukla for their insightful comments. We are thankful for the kind invitation to contribute to a special issue that recognizes the achievements, enthusiasm, and commitment of Ralf Littke. His continued support of our research and his meticulous supervision of the geochemical analyses presented here have been much appreciated. The advice and critical support of Kevin J. Edwards of the Universities of Aberdeen and Cambridge was invaluable in the production of this manuscript.

Data availability All data generated or analyzed during this study are included in this published article.

Declarations

Conflict of interests The authors declare that they have no known competing financial interests or personal relationships that could have appeared to influence the work reported in this paper.

References

- Abdel-Kireem MR, Schrank E, Samir AM, Ibrahim MIA (1996) Cretaceous palaeoecology, palaeogeography and palaeoclimatology of the northern Western Desert. *Egypt J Afr Earth Sci* 22:93–112
- Ahmed MAA (2008) Geodynamic Evolution and Petroleum System of Abu Gharadig Basin, North Western Desert, Egypt (No. RWTH-CONV-113041). *Lehrstuhl für Geologie, Geochemie und Lagerstätten des Erdöls und der Kohle*, p 255
- Arai M, Botelho Neto J, Cunha Lana C, Pedrão E (2000) Cretaceous dinoflagellate provincialism in Brazilian marginal basins. *Cretac Res* 21:351–366
- ASTM D2797/D279, 2021. Standard Practice for Preparing Coal Samples for Microscopical Analysis by Reflected Light. D2797/D279. PA, USA: Am. Soc. Test. Mater, 2021. https://www.astm.org/d2797_d2797m-20.html
- Awad GhM (1984) Habitat of oil in Abu Gharadig and Faiyum Basins, Western Desert. *Egypt AAPG Bull* 68:564–573
- Balme BE (1995) Fossil in situ spores and pollen grains: an annotated catalogue. *Rev Palaeobot Palynol* 87:81–323
- Batten DJ (1996) Palynofacies and palaeoenvironmental interpretation. In: Jansonius J, McGregor DC (eds) *Palynology: Principles and Applications*, vol. 3. AASP Foundation, Dallas (TX), pp 1011–1064
- Batten DJ, Collinson ME, Knobloch E (1994) *Ariadnaesporites* and *Capulisporites*: “water fern” megaspores from the Upper Cretaceous of Central Europe. *Rev Palaeobot Palynol* 83:159–174
- Bayoumi T (1996) The influence of interaction of depositional environment and synsedimentary tectonics on the development of some Late Cretaceous source rocks, Abu Gharadig Basin, Western Desert, Egypt. *Proceedings of 13th Petroleum Exploration and Production Conference, The Egyptian General Petroleum Corporation, EGPC, Cairo, 2: 475–496*
- Bayoumi AI, Lotfy HI (1989) Modes of structural evolution of Abu Gharadig Basin, Western Desert of Egypt as deduced from seismic data. *J Afr Earth Sc* 9:273–287
- Behar F, Beaumont V, Penteado HLD (2001) Rock-Eval 6 technology: Performances and developments. *Oil Gas Sci Technol - Rev IFP Energies Nouvelles* 56(2):111–134. <https://doi.org/10.2516/ogst:2001013>
- Bourbonniere RA, Meyers PA (1996) Sedimentary geolipid records of historical changes in the watersheds and productivities of Lakes Ontario and Erie. *Limnol Oceanogr* 41(2):352–359. <https://doi.org/10.4319/lo.1996.41.2.0352>
- Bray EE, Evans ED (1961) Distribution of Normal-Paraffins as a clue to recognition of source beds. *Geochim Cosmochim Acta* 22(1):2–15. [https://doi.org/10.1016/0016-7037\(61\)90069-2](https://doi.org/10.1016/0016-7037(61)90069-2)
- Burnaz L, Zieger L, Schmatz J, Botero AE, Amberg S, Thüms N, Littke R (2023) Preparation techniques for microscopic observation of dispersed organic matter and their effect on vitrinite reflectance. *Int J Coal Geol* 272:104249. <https://doi.org/10.1016/j.coal.2023.104249>
- Deaf AS, Harding IC, Marshall JEA (2020) Cretaceous (Hauterivian-Cenomanian) palaeoceanographic conditions in southeastern Tethys (Matruh Basin, Egypt): implications for the Cretaceous climate of northeastern Gondwana. *Cretac Res* 106:104229
- Didyk BM, Simoneit BRT, Brassell SC, Eglinton G (1978) Organic geochemical indicators of palaeoenvironmental conditions of sedimentation. *Nature* 272:216–222
- Dominik W (1985) Stratigraphie und Sedimentologie (Geochemie, Schwermineralanalyse) der Oberkreide von Bahariya und ihre Korrelation zum Dakhla-Becken (Western Desert, Ägypten). *Berliner Geowissenschaftliche Abhandlungen A* 62:1–173
- El Atfy H (2021) Palynofacies as a paleoenvironment and hydrocarbon source potential assessment tool: an example from the

- Cretaceous of north Western Desert. Egypt Palaeobiodiversity and Palaeoenvironments 101:35–50
- El Atfy H, Anan T, El-Soughier MI (2017) Paleoeologic and stratigraphic significance of the freshwater algae *Pediastrum* in the Upper Cretaceous (Turonian) marine deposits, north Western Desert. Egypt Palz 91:273–281
- El Atfy H, Ghassal BI, Littke R (2023a) Petroleum source rocks of Egypt: an integrated spatio-temporal palynological and organic geochemical studies within the phanerozoic. In: Hamami Z et al. (eds). The Phanerozoic Geology and Natural Resources of Egypt. Advances in Science Technology & Innovation. Springer, Cham, pp 649–674. https://doi.org/10.1007/978-3-030-95637-0_23
- El Atfy H, Coiffard C, El Bealy S, Uhl D (2023b) Vegetation and climate change at the southern margin of the Neo-Tethys during the Cenomanian (Late Cretaceous): evidence from Egypt. PLoS ONE 18(1):0281008
- El Atfy H, Kora M, Soliman A, Kassem AA, Said S, Aboulsaud A, El Desouky H, Bomfleur B (2023c) New insights into Coniacian-Santonian palynology in the Neo-Tethys (Egypt), with special emphasis on the ecological and depositional significance of the freshwater alga *Pediastrum*. J Afr Earth Sc 205:105006
- El Bealy SY, El Atfy HS, Zavada MS, El Khoriby EM, Abu-Zied RH (2010a) Palynological, palynofacies, paleoenvironmental and organic geochemical studies on the Upper Cretaceous succession of the GPTSW-7 well, North Western Desert Egypt. Marine Petrol Geol 27:370–385
- El Bealy SY, Head MJ, El Atfy HS (2010b) Palynology of the Mid-Cretaceous Malha and Galala formations, Gebel El Minshera, north Sinai Egypt. PALAIOS 25:517–526
- ELhossainy MM, El-Shafeiy M, Al-Areeq NM, Hamdy D (2022) Petroleum generation modelling of the Middle-Late Cretaceous sediments in the Abu Gharadig Field, northwestern Desert Egypt. Geol J 57:3851–3880
- Evenick JC (2021) Examining the relationship between Tmax and vitrinite reflectance: an empirical comparison between thermal maturity indicators. J Nat Gas Sci Eng 91:103946
- Gastaldo RA (1994) The genesis and sedimentation of phytoclasts with examples from coastal environments. In: Traverse A (ed) Sedimentation of Organic Particles. Cambridge University Press, pp 103–128
- Ghassal BI, El Atfy H (2023) Sedimentary organic matter: origin, productivity, preservation, and role in source rock development. In: El Atfy H, Ghassal BI (eds) Advances in petroleum source rock characterizations: integrated methods and case studies advances in science technology & innovation. Springer, Cham, pp 3–22
- Ghassal BI, Littke R, El Atfy H, Sindern S, Scholtysik G, El Bealy S, El Khoriby E (2018) Source rock potential and depositional environment of Upper Cretaceous sedimentary rocks, Abu Gharadig Basin, Western Desert, Egypt: an integrated palynological, organic and inorganic geochemical study. Int J Coal Geol 186:14–40
- Ghassal BI, Mutairi SS, El Atfy H (2023) Practical guide for petroleum source rock interpretation. In: El Atfy H, Ghassal BI (eds) Advances in Petroleum Source Rock Characterizations: Integrated Methods and Case Studies Advances in Science, Technology & Innovation. Springer, Cham, pp 25–45
- Grohmann S, Fietz SW, Littke R, Daher SB, Romero-Sarmiento MF, Nader FH, Baudin F (2018) Source rock characterization of Mesozoic to Cenozoic organic matter rich marls and shales of the Eratosthenes Seamount, Eastern Mediterranean Sea. Oil Gas Sci Technol Revue d'IFP Energies Nouvelles 73:49
- Guiraud R, Bosworth W (1999) Phanerozoic geodynamic evolution of northeastern Africa and the northwestern Arabian platform. Tectonophysics 315:73–108
- Guiraud R, Issawi B, Bosworth W (2001) Phanerozoic history of Egypt and surrounding areas. In: Ziegler PA, Cavazza W, Robertson AHF, Crasquin-Soleau S (eds) Peri-Tethys Memoir 6: Peri-Tethyan Rift/Wrench Basins and Passive Margins. Mémoires du Muséum National d'Histoire Naturelle, Paris, pp 469–509
- Guiraud R, Bosworth W, Thierry J, Delplanque A (2005) Phanerozoic geological evolution of Northern and Central Africa: an overview. J Afr Earth Sc 43:83–143
- Hantar G (1990) North Western Desert. In: Said R (ed) The Geology of Egypt. Balkema, Rotterdam, pp 293–319
- Hartkopf-Fröder C, Königshof P, Littke R, Schwarzbauer J (2015) Optical thermal maturity parameters and organic geochemical alteration at low grade diagenesis to anchimetamorphism: a review. Int J Coal Geol 150–151:74–119
- Huang WY, Meinschein WG (1979) Sterols as ecological indicators. Geochimica et Cosmochimica Acta 43(5):739–745. [https://doi.org/10.1016/0016-7037\(79\)90257-6](https://doi.org/10.1016/0016-7037(79)90257-6)
- Huc AY (1988) Sedimentology of organic matter. In: Frimmel FH, Christman RF (eds) Humic substances and their role in the environment. John Wiley & Sons, London, pp 215–243
- Hunt JM (1996) Petroleum Geochemistry and Geology. W.H. Freeman and Company, New York
- ISO 7404–2, 2009a. Methods for the petrographic analysis of coals - Part 2: Methods of preparing coal samples 7404–2. <https://www.iso.org/standard/42798.html>
- ISO 7404–5, 2009b. Methods for the petrographic analysis of coals - Part 5: Method of determining microscopically the reflectance of vitrinite 7404–5. <https://www.iso.org/standard/42832.html>
- Jarvie DM (1991) Total Organic Carbon (TOC) Analysis. In: Merrill RK (ed) Treatise of Petroleum Geology. Handbook of Petroleum Geology, Source and Migration Processes and Evaluation Techniques, AAPG Press, Tulsa, pp 113–118
- Kerp H, Bomfleur B (2011) Photography of plant fossils — New techniques, old tricks. Rev Palaeobot Palynol 166:117–151
- Mahmoud MS, Soliman HA, Deaf AS (2007) Early Cretaceous (Aptian-Albian) palynology of the Kabrit-1 borehole, onshore northern Gulf of Suez. Egypt Revista Española De Micropaleontología 39:169–187
- Marshall JEA, Yule BL (1999) Spore colour measurement. In: Jones TP, Rowe NP (eds) Fossil plants and spores: Modern techniques. The Geological Society, London, pp 165–168
- Mendonça Filho JG, Menezes TR, Mendonça JO, Oliveira AD, Silva TF, Rondon NF, Silva FS (2012) Organic facies: palynofacies and organic geochemistry approaches. In: Panagiotaras D (ed) Geochemistry Earth's system processes. Patras, InTech, pp 211–245
- Moldowan JM, Seifert WK, Gallegos EJ (1985) Relationship between petroleum composition and depositional environment of petroleum source rocks. AAPG Bull 69(8):1255–1268
- Moustafa AR, Saoudi A, Moubasher A, Ibrahim IM, Molokhia H, Schwartz B (2003) Structural setting and tectonic evolution of the Bahariya Depression, Western Desert, Egypt. Georabia 8(1):91–124
- Pearson DL (1984) Pollen/spore color “standard”. Phillips Petroleum Company exploration projects section (reproduction in Traverse 2007). Paleopalynology, Figure 19.2. Springer
- Peters KE (1986) Guidelines for evaluating petroleum source rock using programmed pyrolysis. AAPG Bull 70(3):318–329. <https://doi.org/10.1306/94885688-1704-11D7-8645000102C1865D>
- Peters KE, Walters CC, Moldowan JM (2005) The biomarker guide (Vol. 2). Cambridge University Press, (p 1155)
- Riding JB (2021) A guide to preparation protocols in palynology. Palynology 45(S1):1–110
- Rubinstein I, Sieskind O, Albrecht P (1975) Rearranged sterenes in a shale - occurrence and simulated formation. J Chem

- Society-Perkin Trans 1(19):1833–1836. <https://doi.org/10.1039/p19750001833>
- Said R (1990) Cretaceous paleogeographic maps. In: Said R (ed) *The Geology of Egypt*. Balkema, Rotterdam, pp 439–449
- Shanmugam G (1985) Significance of coniferous rain forest and related organic matter in generating commercial quantities of oil, Gippsland Basin, Australia. *AAPG Bull* 69:1241–1254
- Sinninghe Damsté JS, Kenig F, Koopmans MP, Köster J, Schouten S, Hayes JM, de Leeuw JW (1995) Evidence for gammacerane as an indicator of water column stratification. *Geochim Cosmochim Acta* 59(9):1895–1900
- Slater SM, Wellman CH (2016) Middle Jurassic vegetation dynamics based on quantitative analysis of spore/pollen assemblages from the Ravenscar Group, north Yorkshire. *UK Palaeontology* 59(2):305–328
- Staplin FL (1969) Sedimentary organic matter, organic metamorphism, and oil and gas occurrence. *Bull Can Pet Geol* 17:47–66
- Țabără D, Vasile Ș, Csiki-Sava Z, Bălc R, Vremir M, Chelariu M (2022) Palynological and organic geochemical analyses of the Upper Cretaceous Bozeș Formation at Petrești (southwestern Transylvanian Basin) – biostratigraphic and palaeoenvironmental implications. *Cretac Res* 134:105148
- Thompson CL, JrH D (1986) Optical characteristics of amorphous kerogens and hydrocarbon-generating potential of source rocks. *Int J Coal Geol* 6:229–249
- Tyson RV (1989) Late Jurassic palynofacies trends, Piper and Kimmeridge Clay Formations, UK onshore and offshore. In: Batten DJ, Keen MC (eds) *Northwest European Micropalaeontology and Palynology*. Ellis Horwood, British Micropalaeontological Society Series, pp 135–172
- Tyson RV (1995) Sedimentary organic matter — Organic facies and palynofacies. Chapman and Hall, London, p 615
- Uwins PJR, Batten DJ (1988) Early to Mid-Cretaceous palynology of northeast Libya. In: El Arnauti A, Owens B, Thusu B (eds) *Subsurface palynostratigraphy of North East Libya*. Garyounis University Publication, pp 215–258
- Vajda V, McLoughlin S (2005) A new Maastrichtian-Paleocene *Azolla* species from Bolivia, with a comparison of the global record of coeval *Azolla* microfossils. *Alcheringa* 29(2):305–329
- Vallati P, Tomas AD, Casal G, Calo M (2017) Salviniales from the Late Cretaceous of the Golfo San Jorge basin. *Cretac Res* 74:45–55
- van de Schootbrugge B, Koutsodendris A, Taylor W, Weston F, Wellman C, Strother PK (2024) Recognition of an extended record of euglenoid cysts: implications for the end-Triassic mass extinction. *Rev Palaeobot Palynol* 322:105043
- Zobaa MK, Oboh-Ikuenobe FE, Ibrahim MI (2011) The Cenomanian/Turonian oceanic anoxic event in the Razzak Field, north Western Desert, Egypt: Source rock potential and paleoenvironmental association. *Mar Pet Geol* 28:1475–1482

Springer Nature or its licensor (e.g. a society or other partner) holds exclusive rights to this article under a publishing agreement with the author(s) or other rightsholder(s); author self-archiving of the accepted manuscript version of this article is solely governed by the terms of such publishing agreement and applicable law.